

Hedging Cryptos with Bitcoin Futures

Francis Liu*

Natalie Packham†

Meng-Jou Lu ‡

Wolfgang Karl Härdle§¶

This version: December 22, 2022

Abstract

The introduction of derivatives on Bitcoin enables investors to hedge risk exposures in cryptocurrencies. Because of volatility swings and jumps in cryptocurrency prices, the traditional variance-based approach to obtain hedge ratios is infeasible. As a consequence, we consider two extensions of the traditional approach: first, different dependence structures are modelled by different copulae, such as the Gaussian, Student-t, Normal Inverse Gaussian and Archimedean copulae; second, different risk measures, such as value-at-risk, expected shortfall and spectral risk measures are employed to find the optimal hedge ratio. Extensive out-of-sample tests in the time period December 2017 until May 2021 give insights in the practice of hedging various cryptos and crypto indices, including Bitcoin, Ethereum, Cardano, the CRIX index and a number of crypto-portfolios. Evidence shows that BTC futures can effectively hedge BTC and BTC-involved indices. This promising result is consistent across different risk measures and copulae except for the Frank copula. On the other hand, we observe complex and diverse dependence structures between non-BTC-related cryptoassets and the BTC futures. As a consequence, the hedge performance of non-BTC-related cryptoassets is mixed and even infeasible for some assets.

JEL classification: G11, G13

Keywords: Cryptocurrencies, risk management, hedging, copulas

*Department of Business and Economics, Berlin School of Economics and Law, Badensche Str. 52, 10825 Berlin, Germany. Blockchain Research Center, Humboldt-Universität zu Berlin, Germany. International Research Training Group 1792, Humboldt-Universität zu Berlin, Germany. E-mail: Francis.Liu@hwr-berlin.de.

†Department of Business and Economics, Berlin School of Economics and Law, Badensche Str. 52, 10825 Berlin, Germany. International Research Training Group 1792, Humboldt-Universität zu Berlin, Germany. E-mail: packham@hwr-berlin.de.

‡Department of Finance, Asia University, 500, Lioufeng Rd., Wufeng, Taichung 41354, Taiwan Department of Finance, Asia University, 500, Lioufeng Rd., Wufeng, Taichung 41354, Taiwan E-mail: mangrou@gmail.com.

§Blockchain Research Center, Humboldt-Universität zu Berlin, Germany. Wang Yanan Institute for Studies in Economics, Xiamen University, China. Sim Kee Boon Institute for Financial Economics, Singapore Management University, Singapore. Faculty of Mathematics and Physics, Charles University, Czech Republic. National Yang Ming Chiao Tung University, Taiwan. E-mail: haerdle@wiwi.hu-berlin.de.

¶Financial support of the European Union’s Horizon 2020 research and innovation program “FIN-TECH: A Financial supervision and Technology compliance training programme” under the grant agreement No 825215 (Topic: ICT-35-2018, Type of action: CSA), the European Cooperation in Science & Technology COST Action grant CA19130 - Fintech and Artificial Intelligence in Finance - Towards a transparent financial industry, the Deutsche Forschungsgemeinschaft’s IRTG 1792 grant, the Yushan Scholar Program of Taiwan and the Czech Science Foundation’s grant no. 19-28231X / CAS: XDA 23020303, and DFG IRTG 1792 gratefully acknowledged.

Contents

1	Introduction	3
2	Optimal hedge ratio	4
2.1	Distribution of hedge portfolio	4
2.2	Backtesting Procedure	7
3	Copulae	8
3.1	Gaussian and t Copulae	8
3.2	Archimedean copulae	9
3.3	Mixture Copula	10
3.4	NIG factor copula	11
3.5	Plackett copula	13
3.6	Calibration	13
3.7	Copula selection	14
4	Risk measures	15
5	Empirical Results	16
5.1	Data	17
5.2	Overview of the out-of-sample data	17
5.3	An overview of the hedged portfolios without the copula selection step	21
5.4	Copula Selection Results	23
5.5	Hedged portfolios with the copula selection step	24
5.6	Hedging Effectiveness Results	24
6	Conclusion and Outlook	27
A	Density of linear combination of random variables	32
B	Summary Statistics	33
C	Supplementary Material: Intraday Hedging	37

1 Introduction

Cryptocurrencies (CC's) are a fast-growing asset class, with many more CCs now available on the market since the first cryptocurrency Bitcoin (BTC) surfaced (Nakamoto, 2009). In response to the rapid development of the CC market, the CME Group launched exchange-traded BTC futures contracts in December 2017. At the time of writing, the CME Bitcoin futures is one of a few crypto futures that is available on regulated exchange that offers regulated crypto futures ¹. As per the CME report on 25th of Nov, 2022, the average daily volume and open interest of the CME BTC futures are \$1,220M and \$1,357M respectively ². Because it is regulated, the CME BTC derivatives market is an attractive way for institutional investors to participate in or manage their exposure in the crypto market. As more individual and institutional investors are adding CCs and CC derivatives to their portfolios, the need to understand downside risks and find suitable ways to hedge against extreme risks is created. From a risk management perspective, the roller-coaster ride of crypto prices may create significant basis risk, even when using simple hedges involving crypto portfolios and BTC futures. This requires analysing the dependence structure of cryptos and futures beyond linear correlation.

In this paper, we examine hedges of crypto portfolios with Bitcoin futures. Owing to the asymmetry of crypto returns as well as the occurrence of extreme events, we consider different dependence structures via a variety of copula models. We then optimise the hedge ratio using different risk measures. A similar study was conducted by (Barbi and Romagnoli, 2014) for equity and FX portfolios. Barbi and Romagnoli (2014)'s work is based on Cherubini et al. (2011) to derive the distribution of linear combinations of margins with copulae describing the dependence structure. We slightly extend their results and come up with a formula for the linear combination of random variables for our purpose.

The hedge ratio is the appropriate amount of futures contracts to hold in order to eliminate the risk exposure in the underlying security. The determination of the optimal hedge ratio relies primarily on the dependence between BTC and futures prices. Financial asset returns have long known to be non-Gaussian, see e.g. (Fama, 1963; Cont, 2001). Specifically, Gaussian models cannot produce the heavy tails and the asymmetry observed in asset returns, which in turn implies a consistent underestimation of financial risks. Therefore, to minimize downside risk, one cannot solely rely on second-order moment calculations. Moreover, variance as a risk measure does not account for the variety of investors' utility functions. In particular, it is known that investors are tail-risk averse, see Menezes et al. (1980). Copulae provide the flexibility to model multivariate random variables separately by their margins and dependence structure. The concept of copulae was originally developed (but not under this name) by Wassily Hoeffding (Hoeffding, 1940a) and later popularised by the work of Abe Sklar (Sklar, 1959).

Different risk measures account for investors' risk attitudes. They serve as loss functions in the search process of the optimal hedge ratio. Of the vast literature discussing the relationship between risk measures and investors' risk attitudes, we refer readers to Artzner et al. (1999) for an axiomatic approach of risk measure construction; Embrechts et al. (2002) for reasoning of using expected shortfall (ES) and spectral risk measures (SRM) in addition to value-at-risk (VaR); Acerbi (2002) for direct linkages between risk measures and investor's risk attitudes using the concept of a "risk aversion function".

In order to capture a variety of risk preferences, in addition to variance, we include the risk measures


¹We thank the referees for reminding the authors that Bakkt BTC futures are also available on regulated exchange.

²Data from CME: https://www.cmegroup.com/ftp/bitcoinfutures/Bitcoin_Futures_Liquidity_Report_20221202.pdf

value-at-risk (VaR), expected shortfall (ES), and spectral risk measures (SRM). VaR is widely used by the finance industry and easy to understand. ES and SRM are chosen because of their coherence property, in particular, they recognize diversification benefits. SRM can also be directly related to an individual's utility function. Examples are the exponential SRM and power SRM introduced by Dowd et al. (2008).

Evaluating the hedging effectiveness of crypto derivatives has been done by many researchers. Deng et al. (2020) show that the crypto inverse futures is able to be used to hedge against BTC exposure. Alexander et al. (2020) crypto derivatives on BitMEX not only play an important role in price discovery of BTC, they can be used as hedging instrument to offset the movement of BTC price. Sebastião and Godinho (2020) present promising results of using BTC futures to hedge BTC and other CCs. Alexander et al. (2021) extend the analysis to include the present of liquidation procedure in crypto exchanges. They show that hedgers are able to manage the liquidation probability while keeping a reasonable hedging capability from crypto derivatives.

In this work, we study the effectiveness of hedging various CC's and crypto indices using BTC futures under copula models and different risk preferences. In an extensive backtest,³ we find the ability of the BTC futures to hedge BTC and BTC-related indices promising, regardless of the choices of the copula (with the exception of the Frank copula) and risk measure. On the other hand, the ability of BTC futures to hedge other cryptos and crypto indices is affected by idiosyncratic factors such as regulatory factors and operational risk, but the overall CEM BTCF hedging effectiveness to other cryptos and crypto indices is far lower than that to BTC. We discuss the characteristics of the hedged portfolios constructed by range of risk measures-copulae pairs.

The paper is organized as follows. Section 2 introduces the notion of an optimal hedge ratio as well as the backtesting procedure deployed in this work; Section 3 presents the copulae used in this work as well as the calibration procedure; Section 4 provides the risk measures; Section 5 discusses the backtesting results; Finally, Section 5 concludes the findings. All calculations in this work can be reproduced with the data and code available at www.quantlet.com .

2 Optimal hedge ratio

2.1 Distribution of hedge portfolio

We form a portfolio with two assets, consisting of one unit in the spot asset and a short position of h units of a futures contract, for example one Bitcoin and a short position in a CME Bitcoin futures contract. The objective is to minimize the risk of the exposure in the spot. Let R^S and R^F be the (discrete) returns of the spot and futures price. The (discrete) return of the portfolio is⁴

$$R^h = R^S - hR^F.$$

To measure risk, we define a risk measure ρ to be a mapping from a financial position or its return, such as R^h , to a real number, which is often interpreted as the amount of money to make the position acceptable (e.g. to a regulator), see e.g. (Föllmer and Schied, 2002). For example, a widely used risk measure is value-at-risk (VaR), which, at the confidence level α , is derived from the $1 - \alpha$ quantile of

³We thank the data provider Tiingo (<https://www.tiingo.com/>) for providing the crypto price data.

⁴In practice, as the nominal investment in the futures is zero, R^F is understood as the return on the notional amount underlying the futures contract. In other words, if both the spot price S_{t-1} and the futures price F_{t-1} are normalised to 1, then the portfolio return will be identical to the portfolio value change $\Delta V = \Delta S - h\Delta F$, where $\Delta S = S_t - S_{t-1}$, etc.

the return distribution.

If the portfolio reduces the risk of the spot position, then we call this a hedge portfolio. An optimal hedge ratio h^* is a parameter that minimizes the risk of the aforementioned portfolio

$$h^* = \underset{h}{\operatorname{argmin}} \rho(R^h).$$

Obviously the cdf and pdf of R^h and the risk measure depend on the joint distribution of R^S and $-hR^F$. However, optimising h according to $f_{R^S, -hR^F}$ is unfavourable since one would need to calibrate the joint pdf $f_{R^S, -hR^F}$ whenever updating h . Another problem of using the joint pdf is that one lacks the flexibility to model the margins separately from the dependence structure. Copulae allow to overcome both of these problems.

The advantage of using copulae is two-fold. First, copulae are invariant under strictly monotone increasing function (Schweizer et al., 1981), a property used in Lemma 1 below. Second, copulae allow us to model the margins and dependence structure separately, a result known as Sklar's Theorem (Sklar, 1959), which is given as Theorem 1 below. See also (Nelsen, 1999; Joe, 1997; McNeil et al., 2005) for Sklar's Theorem and more properties of copulae.

We adapt the definition of a two-dimensional copula from (Nelsen, 1999) as follows.

Definition 2.1 (Bivariate copula) *A bivariate copula is a function $C : [0, 1]^2 \mapsto [0, 1]$ with following properties:*

1. *For every u, v in $[0, 1]$,*

$$C(u, 0) = C(0, v) = 0,$$

$$C(u, 1) = u, \text{ and}$$

$$C(1, v) = v;$$

2. *For every u_1, u_2, v_1, v_2 in $[0, 1]$ such that $u_1 \leq u_2$ and $v_1 \leq v_2$,*

$$C(u_2, v_2) - C(u_2, v_1) - C(u_1, v_2) + C(u_1, v_1) \geq 0.$$

The second property is called 2-non-decreasing. In other words, a two-dimensional copula is the joint cdf of a two-dimensional random vector on a unit square with uniform marginals.

The following Theorem, usually known as the Sklar's Theorem, ensures the existence of copula which "couples" a joint distribution function to its univariate margins (Nelsen, 1999, Theorem 2.3.3.).

Theorem 1 (Hoeffding-Sklar-Theorem) *Let F be a joint distribution function with marginal distributions F_X and F_Y . Then, there exists a copula $C : [0, 1]^2 \mapsto [0, 1]$ such that, for all $x, y \in \mathbb{R}$,*

$$F(x, y) = C\{F_X(x), F_Y(y)\}. \tag{1}$$

If the margins are continuous, then C is unique; otherwise C is unique on the range of the margins.

Conversely, if C is a copula and F_X, F_Y are univariate distribution functions, then the function F defined by (1) is a joint distribution function with margins F_X, F_Y .

Hence, copula enables hedgers to model the dependence structure between the spot and futures separately from their marginals without any restriction imposed by the model assumption marginals.

For example, the marginals of multivariate Gaussian are always Gaussian, but marginals of copula can be any univariate marginals that hedgers flavour. Since we want to focus on the effects of how dependence structure shapes hedging effectiveness, copula allows us to make minimal model assumption on the marginals by deploying kernel density estimators with different bandwidths for the spot and futures.

Regarding the theory behind copula, many basic results can be traced back to early works of Wassily Hoeffding (Hoeffding, 1940b, 1941). The works aimed to derive a measure of relationship of variables, which is invariant under change of scale. See also Fisher and Sen (2012) for English translations of the original papers written in German.

Another feature of copula that is important for hedgers is shown below.

Lemma 1 *Let $h > 0$ and let X and Y be continuous random variables. Then, the joint distribution of the portfolio positions can be expressed via the joint distribution of the securities as follows:*

$$C_{X,hY}(F_X(s), F_{hY}(t)) = C_{X,Y}(F_X(s), F_Y(t/h)), \quad s, t \in \mathbb{R}. \quad (2)$$

Proof. Since copulae are invariant under strictly monotone increasing function Schweizer et al. (1981, Theorem 3 (i)) or Nelsen (1999, Theorem 2.4.3),

$$C_{X,hY}(F_X(s), F_{hY}(t)) = C_{X,Y}(F_X(s), F_{hY}(t)).$$

Re-writing the second argument of the copula gives

$$F_{hY}(t) = \mathbb{P}(hY \leq t) = \mathbb{P}(Y \leq t/h) = F_Y(t/h).$$

■

Lemma 1 describes the fact that copula is invariance under linear transformation. That means rescaling one random variable does not change the dependence structure captured by copula. Searching of optimal hedge ratio (numerically) requires frequent updates of the size of h , but with copula, the search does not require any recalibration. Taking advantage of Lemma 1, Barbi and Romagnoli (2014) introduce the distribution of linear combinations of random variables using copulae. We slightly edit their Corollary 2.1 of their work and yield the following correct expression of the distribution.

Proposition 2 *Let X and Y be two real-valued continuous random variables on a probability space $(\Omega, \mathcal{F}, \mathbf{P})$ with absolutely continuous copula $C_{X,Y}$ and marginal distribution functions F_X and F_Y . Then, the distribution function of $Z = X - hY$, $h > 0$, is given by*

$$F_Z(z) = 1 - \int_0^1 D_1 C_{X,Y} \left[u, F_Y \left\{ \frac{F_X^{(-1)}(u) - z}{h} \right\} \right] du, \quad (3)$$

where, $F^{(-1)}$ denotes the inverse of F , i.e., the quantile function.

Here, $D_1 C(u, v) = \frac{\partial}{\partial u} C(u, v)$ and, see e.g. Equation (5.15) of McNeil et al. (2005),

$$D_1 C_{X,Y}\{F_X(x), F_Y(y)\} = \mathbf{P}(Y \leq y | X = x). \quad (4)$$

Proof. Using the identity (4) gives

$$\begin{aligned} F_Z(z) &= \mathbf{P}(X - hY \leq z) = \mathbb{E} \left\{ \mathbf{P} \left(Y \geq \frac{X - z}{h} \middle| X \right) \right\} \\ &= 1 - \mathbb{E} \left\{ \mathbf{P} \left(Y \leq \frac{X - z}{h} \middle| X \right) \right\} = 1 - \int_0^1 D_1 C_{X,Y} \left[u, F_Y \left\{ \frac{F_X^{(-1)}(u) - z}{h} \right\} \right] du. \end{aligned}$$

■

Corollary 1 *The pdf of Z can be written as*

$$f_Z(z) = h^{-1} \int_0^1 c_{X,Y} \left[F_Y \left\{ \frac{F_X^{(-1)}(u) - z}{h} \right\}, u \right] \cdot f_Y \left\{ \frac{F_X^{(-1)}(u) - z}{h} \right\} du, \quad (5)$$

Note that the pdf of Z in the above proposition can be assessed via numerical integration as long as we have the copula density and the marginal densities. A multivariate generalisation of the expression above and its proof can be found in Appendix A.

2.2 Backtesting Procedure

Time series of out-of-sample hedged portfolio returns that represent a hedger's profit and loss are obtained via the following steps. We start from the earliest 300 data points of each spot-futures pair as training data:

1. **Construct univariate kernel density function (KDE):** Construct the spot and futures' univariate kernel density functions separately using the Gaussian kernel. The bandwidths are determined separately by the refined plug-in method (Härdle et al., 2004, Section 3.3.3).
2. **Calibrate copulae:** Calibrate the copulae outlined in Section 3 by the method of moments described in Section 3.6.
3. **Select copula:** Compute the Akaike Information Criterion (AIC). The copula with the best (i.e. lowest) AIC is used for the next step. A discussion of this step is found in Section 3.7.
4. **Determine optimal hedge ratio:** Determine the optimal hedge ratios with respect to different risk measures numerically. To do so, we draw samples from the calibrated copulae and KDEs and search for the hedge ratio that gives the lowest risk measure. The risk measures are outlined in Section 4. The minimisation algorithm *scipy.optimize.minimize* from the Python package *Scipy* (Virtanen et al., 2020) is used for the search of optimal hedge ratio.
5. **Obtain out-of-sample hedged portfolio returns:** Apply the optimal hedge ratio to the test data to obtain out-of-sample hedged portfolio returns. The test data is the 5 data points subsequent to the last training data point.
6. **Roll forward:** We roll forward by 5 data points and repeat the steps above until the test data reaches the end of the dataset.

The collection of out-of-sample portfolio returns forms a non-overlapping time series since the step size is equal to test data length. The time series represents the profit and loss if hedgers recalibrate

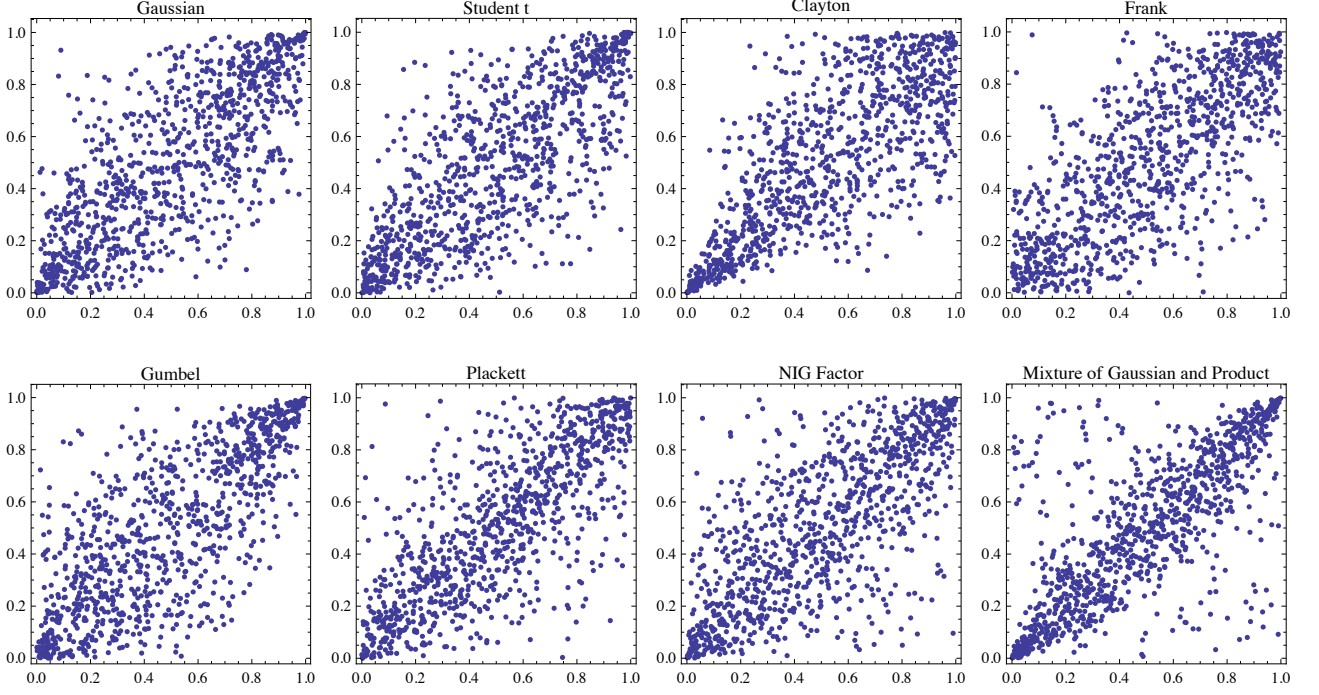


Figure 1: Scatterplots of samples drawn from various copulae. All copulae are calibrated to Spearman's ρ of 0.75 before sampling.

copulae and adjust the hedge ratio every 5 days from the start to the end of the out-of-sample data period. An intraday setup and its results are documented in Appendix C.

The backtesting procedure without the copula selection step (step 3) is also carried out to examine the effects of deploying different copula. Section 5.3 discusses the effects.

3 Copulae

To capture different aspects of the dependence structure between spot and futures, we consider a set of different copulae, they are the Gaussian-, t -, Frank-, Gumbel-, Clayton-, mixture, NIG factor, and Plackett-copula. Figure 1 shows scatter plots of random samples of each of the copulae.

As this hedging exercise concerns only portfolios with two assets, we focus on the bivariate version of each copula.

3.1 Gaussian and t Copulae

The Gaussian and t copulae are derived from Gaussian and t distributions. The bivariate Gaussian copula is defined as

$$C(u, v) = \Phi_{2,\rho}\{\Phi^{(-1)}(u), \Phi^{(-1)}(v)\} \\ = \int_{-\infty}^{\Phi^{(-1)}(u)} \int_{-\infty}^{\Phi^{(-1)}(v)} \frac{1}{2\pi\sqrt{1-\rho^2}} \exp\left\{-\frac{s^2 - 2\rho st + t^2}{2(1-\rho^2)}\right\} ds dt, \quad u, v \in [0, 1],$$

where $\Phi_{2,\rho}$ is the bivariate Normal cdf with zero mean, unit variance, with correlation coefficient ρ , and $\Phi^{(-1)}$ is the quantile function of the univariate standard normal distribution. The Gaussian copula is

fully specified by the correlation parameter ρ .⁵ It has no tail dependence, which, in a finance context, implies that it often underestimates tail risk.

Kendall's τ_K and Spearman's ρ_S of the bivariate Gaussian copula are

$$\tau_K(\rho) = \frac{2}{\pi} \arcsin \rho, \quad \rho_S(\rho) = \frac{6}{\pi} \arcsin \frac{\rho}{2}.$$

The t -copula has the form

$$\begin{aligned} C(u, v) &= \mathbf{T}_{2, \rho, \nu} \{T_\nu^{(-1)}(u), T_\nu^{(-1)}(v)\} \\ &= \int_{-\infty}^{T_\nu^{(-1)}(u)} \int_{-\infty}^{T_\nu^{(-1)}(v)} \frac{\Gamma(\frac{\nu+2}{2})}{\Gamma(\frac{\nu}{2}) \pi \nu \sqrt{1-\rho^2}} \left(1 + \frac{s^2 - 2st\rho + t^2}{\nu}\right)^{-\frac{\nu+2}{2}} ds dt, \end{aligned}$$

where $\mathbf{T}_{2, \rho, \nu}$ denotes the bivariate t cdf with dependence parameter ρ and degrees of freedom parameter ν , $\nu > 2$, and where $T_\nu^{(-1)}(\cdot)$ is the quantile function of a standard t distribution with parameter ν .

The t -copula and Gaussian copula with parameter ρ have equal Kendall's τ , (see Demarta and McNeil, 2005, and references therein). The t -copula has non-zero upper and lower tail dependence, which makes it more appropriate for dependence modelling in finance than the Gaussian copula.

3.2 Archimedean copulae

The family of Archimedean copulae forms a large class of copulae with many convenient features. Archimedean copulas are determined via a simple parametric form of the dependence structure. A prominent feature is the ability to model asymmetric dependence structures.

In general, an Archimedean copula takes the form

$$\mathbf{C}_\theta(u, v) = \psi^{(-1)}\{\psi(u; \theta), \psi(v; \theta); \theta\}, \quad u, v \in [0, 1],$$

where $\psi : [0, 1] \rightarrow [0, \infty)$ is a continuous, strictly decreasing and convex function such that $\psi(1) = 0$ for any permissible dependence parameter θ . The function ψ is called the generator, with $\psi^{(-1)}$ its inverse.

The *Frank copula* (B3 in Joe (1997)) takes the form

$$\mathbf{C}_\theta(u, v) = \frac{1}{\theta} \log \left\{ 1 + \frac{(e^{-\theta u} - 1)(e^{-\theta v} - 1)}{e^{-\theta} - 1} \right\}, \quad u, v \in [0, 1],$$

with $\theta \in [0, \infty]$ the dependence parameter. It is a symmetric copula and cannot produce any tail dependence. The following parameters correspond perfect dependence and independence: $\mathbf{C}_{-\infty} = \mathbf{M}$, $\mathbf{C}_1 = \mathbf{\Pi}$, and $\mathbf{C}_\infty = \mathbf{W}$. The Frank copula has Kendall's τ :

$$\tau_K(\theta) = 1 - 4 \frac{D_1\{-\log(\theta)\}}{\log(\theta)},$$

where D_1 and D_2 are the Debye function of order 1 and 2, with the Debye function defined as $D_n = \frac{n}{x^n} \int_0^x \frac{t^n}{e^t - 1} dt$. We refer readers to Abramowitz and Stegun (1964, p.998) for definition of the Debye function.

⁵The symbol ρ is used to denote both the correlation parameter as well as a general risk measure. However, it will be clear from the context, what ρ refers to.

The *Gumbel copula* (B6 in Joe (1997)) has distribution function

$$\mathbf{C}_\theta(u, v) = \exp - \{(-\log(u))^\theta + (-\log(v))^\theta\}^{\frac{1}{\theta}},$$

where $\theta \in [1, \infty)$ is the dependence parameter. Its Kendall's tau takes the form

$$\tau_K(\theta) = \frac{\theta - 1}{\theta}.$$

It has upper tail dependence with dependence parameter $\lambda^U = 2 - 2^{\frac{1}{\theta}}$ and displays no lower tail dependence.

While the Gumbel copula cannot model perfect counter-dependence (Nelsen, 2002), $\mathbf{C}_1 = \mathbf{\Pi}$ models independence, and $\lim_{\theta \rightarrow \infty} \mathbf{C}_\theta = \mathbf{W}$ models perfect dependence.

The *Clayton copula* takes the form

$$\mathbf{C}_\theta(u, v) = \left\{ \max(u^{-\theta} + v^{-\theta} - 1, 0) \right\}^{-\frac{1}{\theta}},$$

where $\theta \in (-\infty, \infty)$ is the dependence parameter. The Clayton copula, by contrast to Gumbel copula, generates lower tail dependence with $\lambda^L = 2^{-\frac{1}{\theta}}$, but cannot generate upper tail dependence. Moreover, $\lim_{\theta \rightarrow -\infty} \mathbf{C}_\theta = \mathbf{M}$, $\mathbf{C}_0 = \mathbf{\Pi}$, and $\lim_{\theta \rightarrow \infty} \mathbf{C}_\theta = \mathbf{W}$. Kendall's τ of the Clayton copula is given by

$$\tau_K(\theta) = \frac{\theta}{\theta + 2}.$$

3.3 Mixture Copula

The mixture copula is a linear combination of copulae. The distribution of a 2-dimensional random variable $\mathbf{X} = (X_1, X_2)^\top$ is written as linear combination of K copulae

$$\mathbf{C}(u, v) = \sum_{k=1}^K p^{(k)} \cdot \mathbf{C}^{(k)}\{F_{X_1}^{(-1)}(u), F_{X_2}^{(-1)}(v); \boldsymbol{\theta}^{(k)}\}, \quad u, v \in [0, 1].$$

Here, $\boldsymbol{\theta}^{(k)}$ refers to the parameters of the k -th copula.

While Kendall's τ of the mixture copula is not known in closed form, Spearman's ρ is easily derived as

$$\rho_S = \sum_{k=1}^K p^{(k)} \cdot \rho_S^{(k)}.$$

An example of a mixture copula is the Fréchet class of copulae, which are given by convex combinations of \mathbf{W} , $\mathbf{\Pi}$, and \mathbf{M} (Nelsen, 1999).

We use the *Gaussian Mix Independent Copula (GMI)* in our analysis, i.e.,

$$\mathbf{C}(u, v) = p \mathbf{C}_\theta^{\text{Gaussian}}(u, v) + (1 - p)(uv), \quad p \in [0, 1].$$

This mixture models the amount of “random noise” that appears in the off-diagonal region of the dependence structure where the Gaussian copula has no control. In the hedging exercise, the structure of the off-diagonal “random noise” is not our main concern, but the amount of it might affect the hedging effectiveness.

3.4 NIG factor copula

Normal Inverse Gaussian (NIG) distribution is a flexible and yet analytical tractable distribution introduced by (Barndorff-Nielsen, 1997). The *NIG factor copula* is constructed based on the characteristics of the NIG distribution. This section presents the version of NIG factor copula we use in this work. The NIG distribution has density function

$$g(x; \alpha, \beta, \mu, \delta) = \frac{\alpha}{\pi} e^{\delta \sqrt{\alpha^2 - \beta^2} - \beta \mu} \frac{1}{q((x - \mu)/\delta)} K_1 \left[\delta \alpha q \left(\frac{x - \mu}{\delta} \right) \right] e^{\beta x}, \quad x > 0,$$

where $q(x) = \sqrt{1 + x^2}$ and where K_1 is the modified Bessel function of third order and index 1. The parameters satisfy $0 \leq |\beta| \leq \alpha$, $\mu \in \mathbb{R}$ and $\delta > 0$, and have the following interpretation: μ and δ are location and scale parameters, respectively, α determines the heaviness of the tails and β determines the degree of asymmetry. If $\beta = 0$, then the distribution is symmetric around μ .

The cdf and quantile function of NIG distribution, denoted by $G(x; \alpha, \beta, \mu, \delta)$ and $G^{(-1)}(x; \alpha, \beta, \mu, \delta)$, have no known analytical form. In this work, they are computed via numerical integration of the density and by simulation.

The NIG distribution belongs to the class of so-called *normal variance-mean mixture distributions*, (see Section 3.2 of McNeil et al. (2005)): X follows an $NIG(\alpha, \beta, \mu, \delta)$ distribution if X conditional on W follows a normal distribution with mean $\mu + \beta W$ and variance W , i.e.,

$$X|W \stackrel{\mathcal{L}}{\sim} N(\mu + \beta W, W),$$

where W follows an *inverse Gaussian distribution*, denoted by $IG(\delta, \sqrt{\alpha^2 - \beta^2})$.

The simulation procedure of the $NIG(\alpha, \beta, \mu, \delta)$ distribution is a natural result of the above decomposition. To simulate the NIG distribution, first simulate a random variable $w \sim IG(\delta, \sqrt{\alpha^2 - \beta^2})$, then simulate $x \sim N(\mu + \beta w, w|w)$.

The moment-generating function of the NIG distribution is given by

$$M(u; \alpha, \beta, \mu, \delta) = \exp \left(\delta \left(\sqrt{\alpha^2 - \beta^2} - \sqrt{\alpha^2 - (\beta + u)^2} \right) + \mu u \right).$$

As a direct consequence, moments are easily calculated with the expectation and variance of the NIG distribution being

$$\begin{aligned} \mathbb{E}X &= \mu + \frac{\delta \beta}{\sqrt{\alpha^2 - \beta^2}} \\ \text{Var}(X) &= \frac{\alpha^2 \delta}{(\alpha^2 - \beta^2)^{3/2}}. \end{aligned} \tag{6}$$

It is easily seen from the moment-generating function that the NIG distribution is preserved under linear combinations, provided the variables share the parameters α and β .

Proposition 3.1 *Let $Z \sim NIG(\alpha, \beta, \mu, \delta)$ and $Z_i \sim NIG(\alpha, \beta, \mu_i, \delta_i)$, $i = 1, \dots, n$ be independent NIG-distributed random variables. Then:*

1. $X_i = Z + Z_i \sim NIG(\alpha, \beta, \mu + \mu_i, \delta + \delta_i)$,

2. and

$$\begin{aligned} \text{Cov}(X_i, X_j) &= \text{Var}(Z), \\ \text{Corr}(X_i, X_j) &= \frac{\delta}{\sqrt{(\delta + \delta_i)(\delta + \delta_j)}}. \end{aligned} \quad (7)$$

Proof.

1. This follows directly from the moment-generating function.
2. For the covariance,

$$\text{Cov}(X_i, X_j) = \mathbb{E}[(Z + Z_i)(Z + Z_j)] - \mathbb{E}[Z + Z_i]\mathbb{E}[Z + Z_j] = \mathbb{E}[Z^2] - (\mathbb{E}Z)^2.$$

The correlation is determined directly from 6. ■

The NIG distribution is popular in many areas of financial modelling; for example, it gives rise to the normal inverse Gaussian Lévy process, which may be represented as a Brownian motion with a time change. In the setting here, we consider the *NIG factor copula*, which is not directly derived from the multivariate NIG distribution, but determined through a factor structure instead.⁶

(fix delta1 and delta2 but let the delta from Z free; everything is standardised for copula)

The bivariate NIG factor model is given by

$$\begin{aligned} X &= Z + Z_1 \\ Y &= Z + Z_2, \end{aligned}$$

where $Z \sim \text{NIG}(\alpha, \beta, \mu, \delta)$, $Z_1 \sim \text{NIG}(\alpha, \beta, \mu_1, \delta_1)$, $Z_2 \sim \text{NIG}(\alpha, \beta, \mu_2, \delta_2)$, and Z, Z_1, Z_2 are mutually independent.

The following normalising steps reduce the number of parameters to three:

1. Set $\mu = \mu_1 = \mu_2 = 0$. The location parameter does not affect the correlation structure.
2. Set $\delta_1 = \delta_2 = \frac{(\alpha^2 - \beta^2)^{3/2}}{\alpha^2}$ such that Z_1 and Z_2 are unit variance. Normalising the scale parameter does not affect the correlation structure.

The dependence between X and Y is now fully captured by α, β , and δ .

Proposition 3.2 *Let $u, v \in [0, 1]$, $\alpha, \beta \in \mathbb{R}$ satisfying $0 \leq |\beta| \leq \alpha$, $\delta > 0$, $f(\cdot) = g(\cdot; \alpha, \beta, 0, \delta)$, and $F(\cdot) = G(\cdot; \alpha, \beta, 0, \frac{(\alpha^2 - \beta^2)^{3/2}}{\alpha^2})$. The NIG factor copula is*

$$C(u, v) = \int_{\mathbb{R}} F\{F^{(-1)}(u) - z\} F\{F^{(-1)}(v) - z\} f(z) dz.$$

⁶The factor structure, which was applied e.g. in (Kalemanova et al., 2007) for calibrating CDO's, gives additional flexibility as it does not force the components to have a mixing variable W .

Proof. Let F_X and F_Y be the cdfs, $F_X^{(-1)}$ and $F_Y^{(-1)}$ be the quantile functions of X and Y respectively.

$$\begin{aligned}
C(u, v) &= \mathbf{P}(F_X(X) \leq u, F_Y(Y) \leq v) \\
&= \mathbb{E} \{ \mathbf{P}(F_X(X) \leq u, F_Y(Y) \leq v | Z) \} \\
&= \mathbb{E} \left\{ \mathbf{P} \left(Z_1 \leq F_X^{(-1)}(u) - Z, Z_2 \leq F_Y^{(-1)}(v) - Z \mid Z \right) \right\} \\
&= \int_{\mathbb{R}} F \left\{ F^{(-1)}(u) - z \right\} F \left\{ F^{(-1)}(v) - z \right\} f(z) dz.
\end{aligned}$$

■

We refer readers to Krupskii et al. (2018) for the methodology of constructing factor copulae. See also Joe (2014, Section 3.10) and Krupskii and Joe (2013).

The quantile dependence and Spearman's rho of NIG factor copula have no known analytical form. In this work, the quantile dependence is computed numerically; Spearman's rho is approximated by Spearman's rho of the bivariate Gaussian copula. When $\beta \rightarrow 0$ and $\alpha \rightarrow \infty$, the NIG distribution behaves similarly to the Gaussian distribution, making the (bivariate) NIG factor copula behave similarly to the (bivariate) Gaussian copula. Therefore, the NIG factor copula's Spearman's rho is well approximated by the Spearman's rho of the bivariate Gaussian copula.

3.5 Plackett copula

The Plackett copula has distribution function

$$C_\theta(u, v) = \frac{1 + (\theta - 1)(u + v)}{2(\theta - 1)} - \frac{\sqrt{\{1 + (\theta - 1)(u + v)\}^2 - 4uv\theta(\theta - 1)}}{2(\theta - 1)},$$

where $0 \leq \theta < \infty$. Spearman's rho is given by

$$\rho_S(\theta) = \frac{\theta + 1}{\theta - 1} - \frac{2\theta \log \theta}{(\theta - 1)^2}.$$

The Plackett copula possesses a special property: the cross-product ratio is equal to the dependence parameter

$$\frac{\mathbf{P}(U \leq u, V \leq v) \cdot \mathbf{P}(U > u, V > v)}{\mathbf{P}(U \leq u, V > v) \cdot \mathbf{P}(U > u, V \leq v)} = \frac{C_\theta(u, v)\{1 - u - v + C_\theta(u, v)\}}{\{u - C_\theta(u, v)\}\{v - C_\theta(u, v)\}} = \theta.$$

In words, the dependence parameter is equal to the ratio of the number of concordance pairs and the number of discordance pairs of a bivariate random variable.

3.6 Calibration

We trace back the usage of method of moments (MM) to calibrate copulae to Genest (1987); Genest and Rivest (1993) where the moments mainly refer to Kendall's τ or Spearman's ρ . Adapted from Oh and Patton (2013), we extend MM to quantile dependence measures. Quantile dependence is denoted by λ_q for quantile level q .

Spearman's rho ρ_S , Kendall's tau τ_K , and quantile dependence of the copula C are defined as

$$\begin{aligned}\rho_S &= 12 \int \int_{I^2} C_{\boldsymbol{\theta}}(u, v) \, du \, dv - 3 \\ \tau_K &= 4\mathbb{E}[C_{\boldsymbol{\theta}}\{F_X(x), F_Y(y)\}] - 1, \\ \lambda_q &= \begin{cases} \mathbf{P}(F_X(X) \leq q | F_Y(Y) \leq q) = \frac{C_{\boldsymbol{\theta}}(q, q)}{q}, & \text{if } q \in (0, 0.5], \\ \mathbf{P}(F_X(X) > q | F_Y(Y) > q) = \frac{1 - 2q + C_{\boldsymbol{\theta}}(q, q)}{1 - q}, & \text{if } q \in (0.5, 1). \end{cases}\end{aligned}$$

The empirical counterparts are

$$\begin{aligned}\hat{\rho}_S &= \frac{12}{n} \sum_{k=1}^n \hat{F}_X(x_k) \hat{F}_Y(y_k) - 3, \\ \hat{\tau}_K &= \frac{4}{n} \sum_{k=1}^n \hat{C}\{\hat{F}_X(x_k), \hat{F}_Y(y_k)\} - 1, \\ \hat{\lambda}_q &= \begin{cases} \frac{1}{n} \sum_{k=1}^n \frac{\mathbf{1}_{\{\hat{F}_X(x_k) \leq q, \hat{F}_Y(y_k) \leq q\}}}{q}, & \text{if } q \in (0, 0.5], \\ \frac{1}{n} \sum_{k=1}^n \frac{\mathbf{1}_{\{\hat{F}_X(x_k) > q, \hat{F}_Y(y_k) > q\}}}{1 - q}, & \text{if } q \in (0.5, 1), \end{cases}\end{aligned}$$

where $\hat{F}(x) = \frac{1}{n} \sum_{k=1}^n \mathbf{1}_{\{x_i \leq x\}}$ and $\hat{C}(u, v) = \frac{1}{n} \sum_{k=1}^n \mathbf{1}_{\{u_i \leq u, v_i \leq v\}}$.

Denote by $\mathbf{m}(\boldsymbol{\theta})$ the m -dimensional vector of dependence measures according the dependence parameters $\boldsymbol{\theta}$, and let $\hat{\mathbf{m}}$ be the corresponding empirical counterpart. The difference between dependence measures and their counterpart is denoted by

$$\mathbf{g}(\boldsymbol{\theta}) = \hat{\mathbf{m}} - \mathbf{m}(\boldsymbol{\theta}),$$

and the *MM estimator* is

$$\hat{\boldsymbol{\theta}} = \underset{\boldsymbol{\theta} \in \boldsymbol{\Theta}}{\operatorname{argmin}} \mathbf{g}(\boldsymbol{\theta})^\top \hat{\mathbf{W}} \mathbf{g}(\boldsymbol{\theta}),$$

where $\hat{\mathbf{W}}$ is a positive definite weight matrix. In this work, we use $\mathbf{m}(\boldsymbol{\theta}) = (\rho_S, \lambda_{0.05}, \lambda_{0.1}, \lambda_{0.9}, \lambda_{0.95})^\top$ for calibration with $\hat{\mathbf{W}}$ set to the identity matrix. We replace Spearman's rho by Kendall's tau when the analytical form of the former is not available.

While maximum likelihood estimation is a viable procedure to calibrate copula, we choose MM as the estimation procedure in this work. Figure 2 shows the empirical quantile dependence of Bitcoin and CME futures and the copula implied quantile dependence of the MLE and MM calibration procedures. Although the MLE is a better fit to a range of quantile dependence in the middle, it fails to address the situation in the tails.

3.7 Copula selection

As the dependence structure of price data changes across time, we allow for a flexible choice of the best-fitting copula, by re-calibrating periodically and re-evaluating performance of the various copulas. In each re-calibration, we select the best-fitting copula, characterised by the lowest *Akaike*

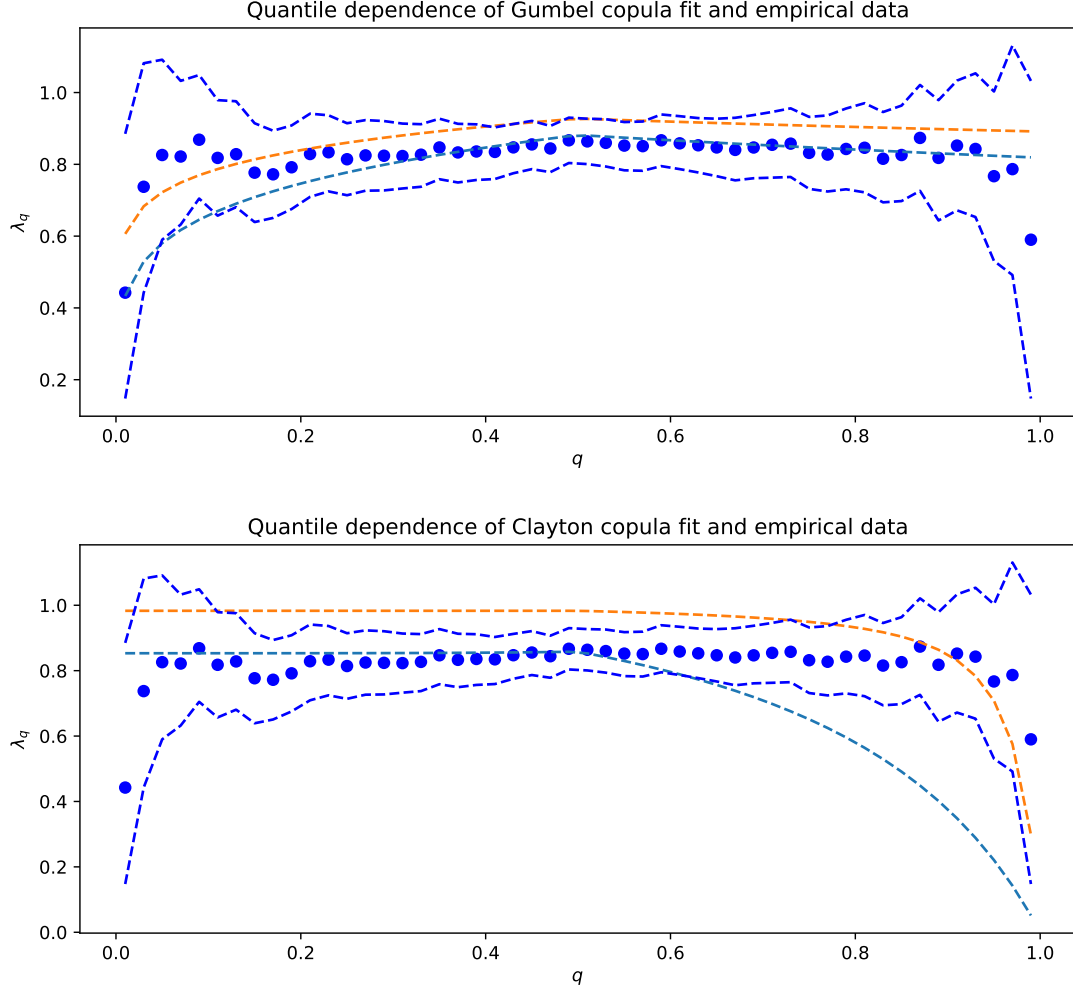


Figure 2: Quantile dependences of Gumbel and Clayton copulas. The blue circle dots are the quantile dependence estimates of Bitcoin and CME future, the blue dashed lines are the estimates' 90% confidence interval. The orange dotted line is the copula implied quantile dependence by MM estimation. The light blue dotted line is the copula implied quantile dependence by MLE estimation.

Information Criterion (AIC),

$$AIC = 2k - 2\log(L),$$

where k is the number of estimated parameters and L is the likelihood (Akaike, 1973).

Other model selection criteria, such as the TIC (Takeuchi, 1976) or likelihood ratio test could be used instead. For a survey of model selection and inference, see Anderson et al. (1998). Among various copula selection procedures, AIC is a popular choice for its applicability, see e.g. Breymann et al. (2003). In our case, the AICs are calculated only with dependence likelihood since the marginals are modelled via kernel density estimators. The selected copula will then enter the calculation of the optimal hedge ratio.

4 Risk measures

The optimal hedge ratio is determined for the following variety of risk measures: variance, Value-at-Risk (VaR), Expected Shortfall (ES), and Exponential Risk Measure (ERM). A summary of risk measures being used in portfolio selection problem can be found in Härdle et al. (2008). The risk

measures here serve as risk minimization objectives, i.e. loss functions for searching the optimal hedge ratio.

The risk measures are defined as follows. Let Z be a random variable with distribution function F_Z .

1. Variance: $\text{Var}(Z) = \mathbb{E}[(Z - \mathbb{E}Z)^2]$.
2. VaR at confidence level α : $\text{VaR}_\alpha(Z) = -F_Z^{(-1)}(1 - \alpha)$
3. ES at confidence level α : $\text{ES}_\alpha(F_Z) = -\frac{1}{1-\alpha} \int_0^{1-\alpha} F_Z^{(-1)}(p) dp$
4. ERM with Arrow-Pratt coefficient of absolute risk aversion k :

$$\text{ERM}_k(Z) = - \int_{[0,1]} \phi(p) F_Z^{(-1)}(p) dp,$$

where ϕ is a weight function described in (4) below.

VaR, ES, and ERM fall into the class of spectral risk measures (SRM), which have the form (Acerbi, 2002)

$$\rho_\phi(Z) = - \int_0^1 \phi(p) F_Z^{(-1)}(p) dp,$$

where p is the loss quantile and $\phi(p)$ is a user-defined weighting function defined on $[0, 1]$. We consider only so-called admissible risk spectra $\phi(p)$, i.e., fulfilling

- (i) ϕ is positive,
- (ii) ϕ is decreasing,
- (iii) and $\int_{[0,1]} \phi(p) dp = 1$.

The VaR's $\phi(p)$ gives all its weight on the $1 - \alpha$ quantile of Z and zero elsewhere, i.e., the weighting function is a Dirac delta function, and hence it violates the (ii) property of admissible risk spectra. The ES' $\phi(p)$ gives all tail quantiles the same weight of $\frac{1}{1 - \alpha}$ and non-tail quantiles zero weight. The ERM assumes investors' risk preference are in the form of an exponential utility function $U(x) = 1 - e^{kx}$, so its corresponding risk spectrum is defined as

$$\phi(p) = \frac{ke^{-k(1-p)}}{1 - e^{-k}},$$

where k is the Arrow-Pratt coefficient of absolute risk aversion. The parameter k has an economic interpretation as being the ratio between the second derivative and first derivative of investor's utility function on a risky asset,

$$k = -\frac{U''(x)}{U'(x)},$$

for x in all possible outcomes. In case of the exponential utility, k is the constant absolute risk aversion (CARA).

5 Empirical Results

5.1 Data

In the empirical analysis, we analyse the capability of CME Bitcoin Futures (BTCF) to reduce the risk of five cryptos, namely Bitcoin (BTC), Ethereum (ETH), Cardano (ADA), Litecoin (LTC) and Ripple (XRP), as well as five crypto indices, namely BITX, BITW100, CRIX, BITW20 and BITW70.

The currencies ETH, ADA, LTC, and XRP are popular cryptos traded at various exchanges and have large market capitalization.

Crypto indices are included in our analysis since they serve as a good proxy for hedgers who need to hedge against a portfolio of cryptos. The indices included are in different numbers of constituents. BITX, BITW100, and CRIX are market-cap weighted crypto indexes with BTC as constituent. BITX and BITW100 track the total return of the 10 and 100 cryptos with largest market-cap, respectively. CRIX determines the number of constituents via AIC and tracks this number of cryptos with largest market-cap. The CRIX index is calculated by the S&P Global and available on Bloomberg ⁷. BITW20 is also a market-cap weighted crypto index but with the 20 largest market-cap cryptos outside the constituents of BITX. BITW70 has the same construction as BITW20 but with the 70 largest market-cap cryptos outside BITX and BITW20. Therefore, BTC is excluded as a constituent in BITW20 and BITW70. All crypto indices are reconstituted monthly to stay updated to the rapidly changing crypto market.

For each of the ten hedge portfolios, a crypto or index is considered as the spot and held in a unit size long position, while the front BTCF is held in a short position with units corresponding to the optimal hedge ratio in order to reduce the risk of the spot. BTCF is rolled over to the next front BTCF after expiry. Except for the hedge of BTC, all hedging portfolios are considered to be cross-asset hedges.

We collect the spots' and BTCF's daily prices at 15:00 US Central Time (CT). The reason for choosing this particular time is that the CME group determines the daily settlements for BTCF's based on the trading activities on CME Globex between 14:59 and 15:00 CT. This is also the reporting time of the daily closing price by Bloomberg. The crypto spot data is collected from the data provider called Tiingo (<https://www.tiingo.com/>). Tiingo aggregates crypto OHLC (open, high, low, and close) prices fed by APIs from various exchanges. It covers major exchanges, such as Binance, Gemini, Poloniex, so Tiingo's aggregated OHLC price is a reasonable representation of a tradable market price. For each crypto, we match the opening price at 15:00 CT from Tiingo with the daily BTCF closing price from Bloomberg. Since CRIX is not available at 15:00 CT, we recalculated an hourly CRIX using the monthly constituents weights and the hourly OHLC price data collected from Tiingo. BITX, BITW20, BITW70, and BITW100 are collected from the official website of their publisher Bitwise.com. The daily reporting time of the Bitwise indexes is 15:00 CT.

The date range of the whole dataset is from 2018-08-13 to 2021-05-27.

5.2 Overview of the out-of-sample data

The date range of the out-of-sample time series is from 2019-10-21 to 2021-05-27, in total of 405 data points in each time series. This section gives an overview of the out-of-sample period.

Figure 3 presents the BTC and BTCF price in USD in the first panel and the difference between the daily returns of BTC and BTCF, i.e. $R_s - R_f$, in the second panel. In the first panel, the black vertical lines with capital letters labels indicate the days of the five most negative daily BTC returns

⁷See <https://www.spglobal.com/spdji/en/custom-indices/royalton-partners-ag-rpag/royalton-crix-crypto-index/#overview>

during out-of-sample period. Table 1 summarizes the relevant news headlines and events of those days.

Figures 4 and 5 show the cumulative returns of the indices and individual cryptos, respectively. The vertical lines labeled by assets name refer to the largest daily price drops of each asset in the out-of-sample data. Table 2 summarises the events that are associated with largest price drops in out-of-sample data.

The out-of-sample data covers the pre-COVID19 period, 2019-10-21 to 2020-03-11 ⁸, as well as the COVID19 period, 2020-03-11 onwards. We observe an overall upward trend of crypto prices in both periods. Nonetheless, the volatilities of assets are high (annualised volatilities are around 100%) regardless of the COVID19 outbreak.

⁸See WHO's announcement in the media briefing on 2020-03-11 <https://www.who.int/director-general/speeches/detail/who-director-general-s-opening-remarks-at-the-media-briefing-on-covid-19---11-march-2020>.



Figure 3: Out-of-sample BTC and BTCF price. The first panel presents the price of BTC in blue line and that of BTCF in orange line. The black vertical lines with capital letter labels indicate the five most negative daily return of BTC in the out-of-sample data. The second panel presents the difference between the percentage returns of BTC and BTCF. The black vertical lines indicate the five most negative returns. The crosses locate the level the returns.

Label	Date	% Drop in Price	Summary
A	2020-03-09	13.83	Coronavirus outbreak that affects the global markets; BTC as potential safe-haven was questioned. ¹
B	2020-03-12	22.89	Continuation of the 2020-03-09 drop.
C	2020-05-11	12.11	Price correction (from \$10,000 to \$8,100) after BTC price surge because of the third supply halving. ^{2,3}
D	2021-01-11	14.41	Short term correction of BTC hits the \$40,000 mark. ⁴
E	2021-05-17	11.86	Tesla stops accepting BTC as payment currency due to environmental concerns related to the excessive energy use in processing transactions. ⁵

Table 1: Summary of events associated with the five most extreme daily price drops in out-of-sample BTC price data. The capital letter labels in the first column correspond to the labels in the first panel of figure 3. ¹ is reported by the CNBC news <https://cnb.cx/3HZ2x7K>; ² is from Forbes <https://bit.ly/3rdJPmP>; ³ is from livemint.com <https://bit.ly/3FRi6Na>; ⁴ is from CNBC <https://cnb.cx/3nU0pp0>; ⁵ is from Reuters <https://reut.rs/3leCiAv>.

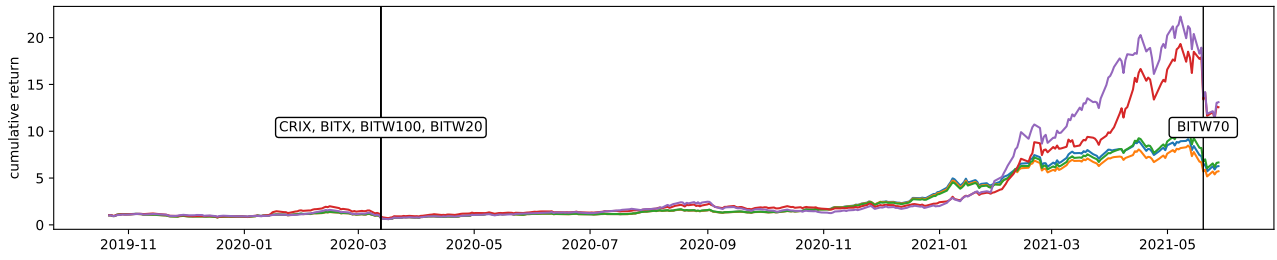


Figure 4: Out-of-sample cumulative returns of crypto indices. The black vertical lines indicate the largest price drops of each index as indicated by the labels. The colouring is as follows: Blue line is CRIX; Orange line is BITX; Green line is BITW100; Red line is BITW20; Purple line is BITW70.

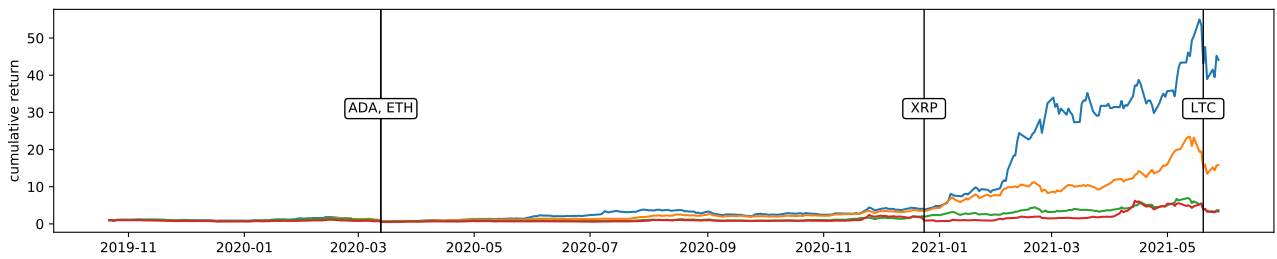


Figure 5: Out-of-sample cumulative returns of individual cryptos. The black vertical lines indicate the largest price drops each cryptos as indicated by the labels. Blue line is ADA; Orange line is ETH; Green line is LTC; Red line is XRP.

Label	Date	% Drop in Price	Summary
CRIX	2020-03-09	23.77	Coronavirus outbreak that affects the global markets including the crypto market.
BITX		23.68	
BITW100		23.87	
BITW20		26.66	
ADA	2020-03-09	23.55	
ETH		27.40	
BITW70		27.64	
XRP	2020-12-23	41.00	Spillover of the BTC shock on 2021-05-17 (label A in Figure 3 and Table 1)
			Top executives of Ripple Labs sued by the SEC of misleading investors ¹ .

Table 2: Summary of events that associated with largest price drops in out-of-sample data. The labels in the first column are the labels in Figure 4 and Figure 5. CRIX, BITX, BITW100, BITW20, ADA and ETH have the same date the reason of the largest drop.¹ is reported by Bloomberg <https://bloom.bg/3cWdita>.

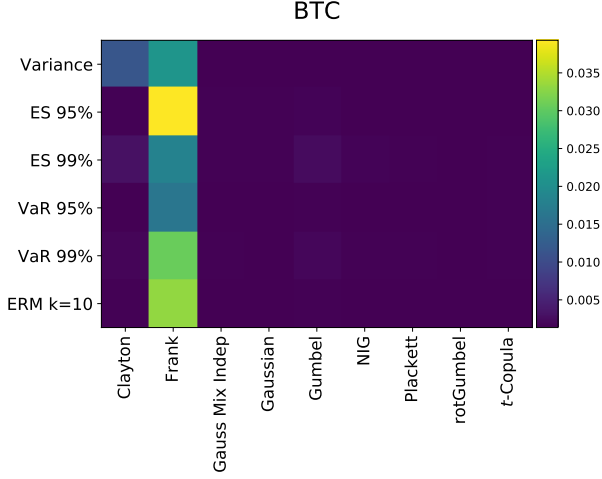


Figure 6: Out-of-sample mean square errors of BTC-BTCF portfolios constructed with different copula and risk minimization objectives. The Frank copula is inferior in the BTC-involved portfolios.

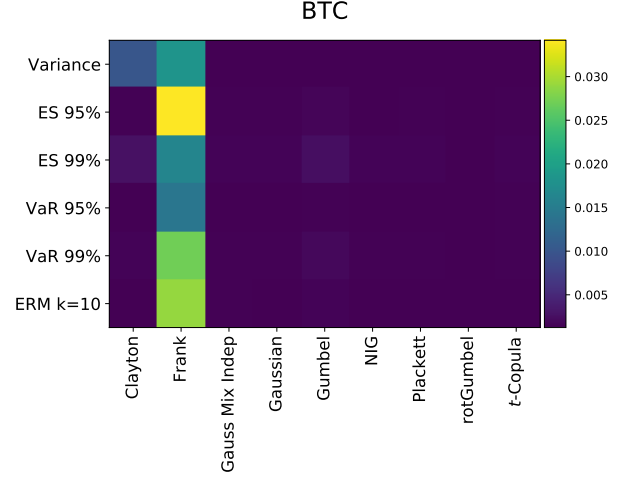


Figure 7: Out-of-sample lower semivariance of BTC-BTCF portfolios constructed with different copula and risk minimization objectives. The Frank copula is obviously inferior.

5.3 An overview of the hedged portfolios without the copula selection step

First, we analyse the results of the hedged portfolios without the copula selection step in order to get a better understanding of how a copula affects the hedged portfolio with various risk minimization objectives. To do so, we inspect the hedge performance of copulas by the mean square error and lower semi-variance. The mean square error is the distance between a perfect hedge and the hedged portfolio returns $MSE = \mathbb{E}(R^2)$. The lower semi-variance is defined as $LSV = \mathbb{E}((R - \mathbb{E}(R))^2 \mathbf{1}_{\{R \leq \mathbb{E}(R)\}})$. All results presented here are out-of-sample results obtained without the copula selection step in order to compare the performances across copulae.

Figures 6 to 11 visualise the out-of-sample MSEs and LSVs of all the portfolios in colorplots. Figures 6 and 7 are the MSEs and LSVs of BTC-BTCF. By far, the Frank copula is the worst performing copula. In Figures 8 and 11, the phenomenon of Frank copula being inferior to its counterparts can also be observed from the results of the CRIX, BITX, BITW100, and BITW20-BTCF portfolios. Interestingly, the spot in those portfolios usually have a strong dependence with the BTCF. In contrast, the inferiority of the Frank copula is less prominent in the BITW70, ADA, ETH, LTC and XRP-BTCF portfolios.

We suspect that the Frank copula is not a choice to model assets with strong dependence.

From Figures 9 and 10, one can see that the Gumbel copula is not performing as well as other copulas in the ETH, LTC, and XRP-BTCF portfolios. The reason is the Gumbel copula has only upper tail dependence, while the ETH, LTC, and XRP exhibit lower tail dependence with BTCF.

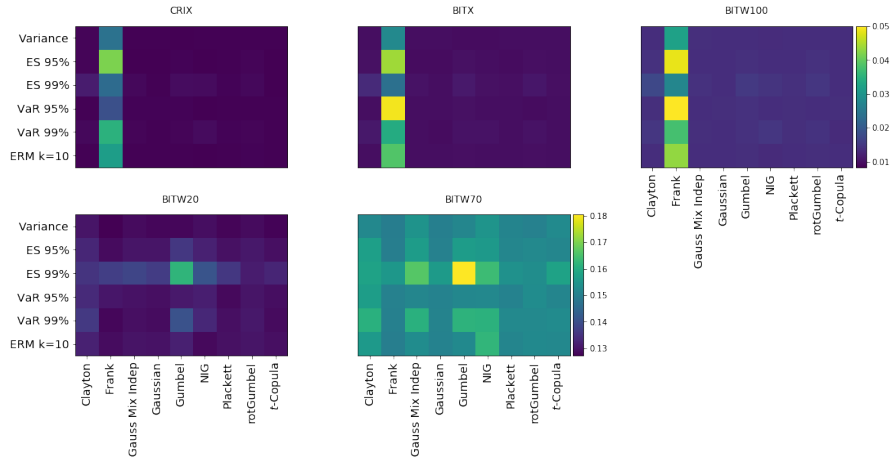


Figure 8: Out-of-sample mean square errors of indices' hedge portfolios. Plots in a row share the same colour scale for comparison.

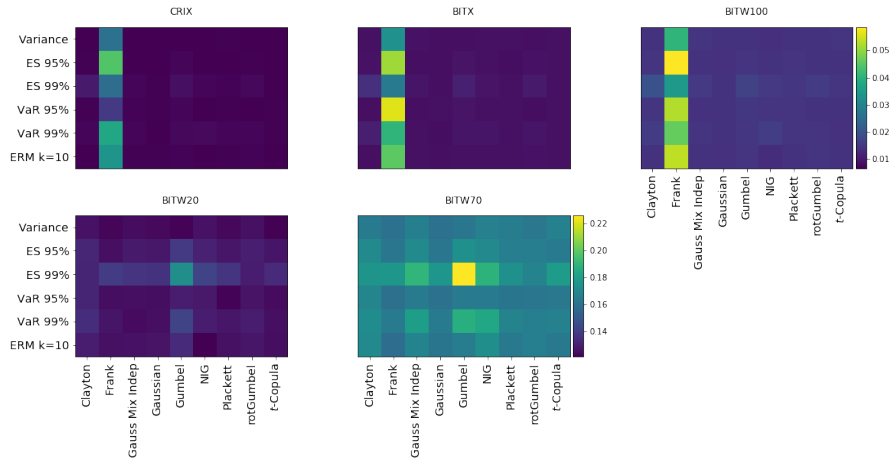


Figure 10: Out-of-sample lower semi variance of indices' hedge portfolios. Plots in a row share the same colour scale for comparison.

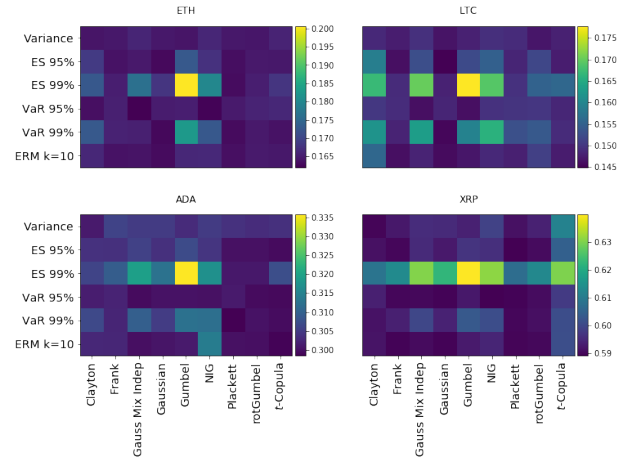


Figure 9: Out-of-sample mean square errors of cryptos' hedge portfolios. Each plot has its own colour scale.

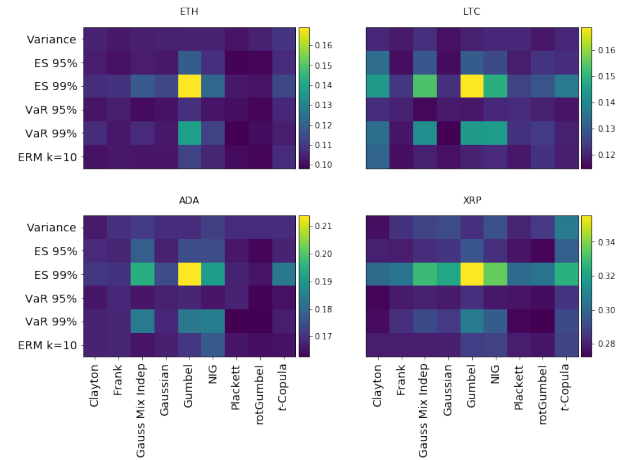


Figure 11: Out-of-sample lower semi variance of cryptos' hedge portfolios. Each plot has its own colour scale.

Spot/ Copula	t	Plackett	GMI	rotGumbel	NIG
Individual Cryptos					
BTC	73	4	2	1	31
ETH	3	6	8	94	1
ADA	0	0	0	0	112
LTC	13	0	3	32	64
XRP	0	31	3	78	0
Crypto Indices with BTC Constituent					
BITX	39	0	14	16	12
CRIX	47	0	11	3	27
BITW100	42	0	8	29	2
Crypto Indices without BTC Constituent					
BITW20	0	0	0	78	3
BITW70	0	0	0	80	1

Table 3: Copula selection results (shortened). The values are the absolute frequencies of a copula chosen by the AIC procedure during the out-of-sample period. Each frequenc represents five trading days, which corresponds to the recalibration interval. The table show the frequently chosen copulas, which are t , Plackett, Gaussian Mix Independent (GMI), rotated Gumbel (rotGumbel) and Normal Inverse Gaussian factor copula (NIG).

5.4 Copula Selection Results

Next, we inspect the copula selection results by the AIC procedure described in Section 3.7. Although the copula selection is only an intermediate step to obtain the optimal hedge ratios, the result of this step can help us better understand the dependence feature between BTCF and the assets we study in this work. This provides valuable information for modeling the assets in the future. The decisions of the AIC procedure are summarised in Table 3. Overall, the t -copula, rotated Gumbel (rotGumbel), and the NIG factor copula are the most frequently chosen copulae by the AIC procedure.

The t -copula is predominantly chosen by the AIC procedure to model the dependence between the BTC and BTC-involving-indices, CRIX, BITX, BITW100, and the BTC future. BTC and BTC-involving-indices exhibit strong (upper and lower) tail dependence with BTCF, a strong tendency for one asset to be extreme when the other is extreme and vice versa. See McNeil et al. (2015) for further details about tail dependence. In fact, the t copula has been recommended in various empirical studies to model financial data, such as Zeevi and Mashal (2002) and Breymann et al. (2003). Those studies suggest that the t -copula is a better model compared to the Gaussian copula as financial data typically exhibit heavy tails and tail dependence.

On the other hand, the symmetric t -copula appears to be a poor choice to model the remaining hedging pairs. Demarta and McNeil (2005) describes the symmetry feature of the t -copula “strong”: if (U_1, \dots, U_d) is a vector distributed in t -copula, then $(U_1, \dots, U_d) \stackrel{\mathcal{L}}{=} (1 - U_1, \dots, 1 - U_d)$.

Here, the AIC criterion predominantly selects copulas that allow for asymmetry between the spot and the BTCF. This reflects that overall asymmetric dependence between a non-BTC-related spot asset and the BTCF. In fact, we observe from the crypto market that asset prices tend to crash simultaneously whereas positive development tends to be idiosyncratic.

Among the three popular copulae, rotGumbel copula shows its ability to model the dependence

between ETH and BTCF. rotGumbel also performs well when modelling dependence between XRP, BITW20, BITW70, and the BTCF. In particular, the whole time series of the two indices, BITW20 and BITW70, are best fitted solely with the rotated Gumbel copula.

In fact, Clayton’s AIC in many of the training sets is the second lowest, just slightly higher than that of rotated Gumbel. This is because the Clayton copula has the same ability to model the lower quantile dependence. However, Clayton’s radial like feature does not match the behaviour of the financial data.

It is worth to mention that although the NIG factor copula is penalised heavily due to its three parameters setup, it is frequently chosen to be the best copula to model the dependence between individual cryptos and the BTC future. An extreme case occurs for ADA, where only the NIG factor is chosen in our dataset. Another dependence structure best described by the NIG factor copula is the pair of LTC-BTCF, with 64 out of 112 training sets best fitted by the NIG factor copula. Indices like BITX and CRIX are sometimes best fitted with the NIG factor copula as well, accounting for modelling 12 and 27 training sets, respectively. The popularity of the NIG factor copula reflects the ability of the copula to model complex dependence structure, involving heavier tails than the Gaussian as well as asymmetric distributions.

The Frank copula turn out to generally be a poor choice to model financial data (as also reported by Barbi and Romagnoli (2014)). The Plackett copula is characterised by its dependence parameter being equal to the cross-product ratio, see (8). However, this property does not capture the dependence structure of cryptos and BTCF.

5.5 Hedged portfolios with the copula selection step

We now turn to the hedge performance. Table 4 presents the first two moments, maximum drawdown (MD) and the date of MD of the hedge portfolios. An interesting observation is the similarity of the statistics when minimising with respect to different risk measures. Detailed statistics are in Tables 6 to 11 in Appendix B.

Unsurprisingly, the BTC-involved spots, i.e., BTC, CRIX, BITX, and BITW100, are well hedged by the BTCF regardless of risk minimization objective. The BTC-not-involved spots, on the contrary, are less promising. Those hedge portfolios’ returns are nearly as volatile as the assets themselves, see for example ADA and XRP. We further discuss the effectiveness of hedge in the next section.

5.6 Hedging Effectiveness Results

In this section, we analyse the out-of-sample hedging effectiveness (HE) of BTCF as a hedge instrument. HE is defined as

$$\text{HE} = 1 - \frac{\rho_h}{\rho_s},$$

i.e., it measures the percentage reduction of risk of the hedge portfolio ρ_h relative to the risk of the spot position ρ_s . A higher HE indicates a greater risk reduction and thus the hedge is more effective. The HE above is a generalisation of how Ederington (1979) evaluates hedge performance, which focusses on variance as the risk measure. Aside from variance, we include the risk measures which act as loss function while searching for the optimal hedge ratios: ES 95% and 99%, VaR 95% and 99% and ERM.

As described in Section 2.2, the backtesting procedure gives an out-of-sample hedged portfolio return time series for every spot-copula-risk measure combination. The time series represent the profit and lost if hedgers recalibrate copulae and adjust the hedge ratio every 5 days. In order to obtain a

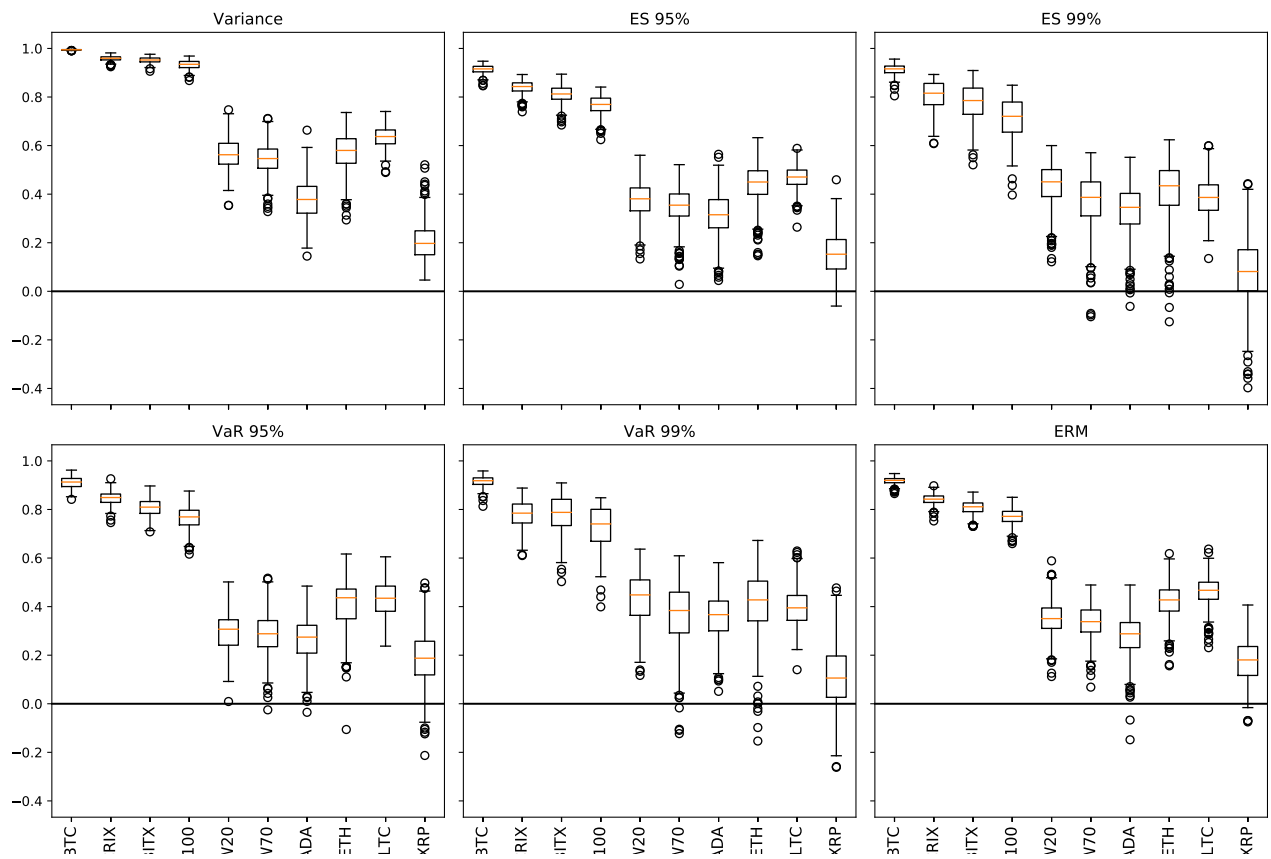



Figure 12: Hedging effectiveness (HE) of portfolios with different risk minimization objectives evaluated by the corresponding risk minimization objectives. The boxplots indicate the the median, upper quartile, lower quartile, minimum and maximum of the bootstrapped HE. The HE of BTC-involved spots are significantly higher than that of BTC-not-involved spots. 

	BTC	ETH	ADA	LTC	XRP	BITX	CRIX	BITW100	BITW20	BITW70
Assets										
Mean %	0.3915	0.6819	0.9467	0.3227	0.2987	0.4308	0.4602	0.4683	0.6249	0.6353
Std %	4.4023	6.0103	6.699	6.4781	7.9843	4.5676	4.542	4.6174	5.5021	5.8155
MD %	-25.9965	-32.0144	-26.8528	-37.5913	-52.7652	-27.022	-27.1385	-27.2694	-31.0092	-32.3453
MD date	2020-03-12	2020-03-12	2020-03-12	2021-05-19	2020-12-23	2020-03-12	2020-03-12	2020-03-12	2020-03-12	2021-05-19
Variance minimizing portfolios										
Mean %	0.0215	0.2823	0.5617	-0.0871	-0.0123	0.0561	0.0812	0.0855	0.2429	0.2706
Std %	0.3221	3.8741	5.2722	3.9052	7.1537	0.9954	0.9183	1.1986	3.5846	3.8838
MD %	-1.4393	-17.7421	-13.8687	-28.3029	-52.5236	-7.7567	-7.1025	-11.3866	-21.468	-23.9984
MD date	2020-11-30	2021-05-19	2021-01-08	2021-05-19	2020-12-23	2021-05-19	2021-05-19	2021-05-19	2021-05-19	2021-05-19
VaR 95% minimizing portfolios										
Mean %	0.0253	0.3084	0.5726	-0.0742	0.0208	0.0562	0.0863	0.0846	0.2728	0.2847
Std %	0.3294	3.8944	5.2204	3.9145	7.152	0.993	0.9151	1.198	3.594	3.9133
MD %	-1.5347	-19.175	-14.6974	-28.3672	-52.5667	-7.5639	-6.9744	-11.2582	-22.0733	-24.6513
MD date	2020-11-30	2021-05-19	2021-05-19	2021-05-19	2020-12-23	2021-05-19	2021-05-19	2021-05-19	2021-05-19	2021-05-19
VaR 99% minimizing portfolios										
Mean %	0.0176	0.2977	0.5562	-0.0852	0.0352	0.0593	0.0738	0.0823	0.2499	0.2788
Std %	0.3270	3.9132	5.3466	4.1503	7.1658	1.0178	0.9695	1.2338	3.621	3.9257
MD %	-1.5689	-18.6061	-15.4795	-29.0915	-52.5727	-8.0299	-7.0185	-11.8752	-21.6634	-24.5294
MD date	2020-11-30	2021-05-19	2021-05-19	2021-05-19	2020-12-23	2021-05-19	2021-05-19	2021-05-19	2021-05-19	2021-05-19
ES 95% minimizing portfolios										
Mean %	0.0204	0.3082	0.5525	-0.0808	0.0176	0.0591	0.0777	0.0848	0.2608	0.2785
Std %	0.3234	3.889	5.2673	3.9829	7.1533	1.0065	0.9207	1.2125	3.6115	3.9157
MD %	-1.5629	-18.7819	-14.9647	-28.4608	-52.5698	-7.6211	-6.9894	-11.1357	-21.543	-24.3474
MD date	2020-11-30	2021-05-19	2021-05-19	2021-05-19	2020-12-23	2021-05-19	2021-05-19	2021-05-19	2021-05-19	2021-05-19
ES 99% minimizing portfolios										
Mean %	0.0148	0.308	0.5016	-0.1029	-0.02	0.0598	0.0835	0.0781	0.2538	0.266
Std %	0.3476	3.8954	5.404	4.1581	7.2887	1.0312	0.9461	1.264	3.6323	3.932
MD %	-1.6225	-18.7625	-15.4481	-29.1727	-52.57	-7.7424	-7.0203	-11.9263	-21.9866	-24.4764
MD date	2020-11-30	2021-05-19	2021-05-19	2021-05-19	2020-12-23	2021-05-19	2021-05-19	2021-05-19	2021-05-19	2021-05-19
ERM $k = 10$ minimizing portfolios										
Mean %	0.0223	0.3117	0.5722	-0.0512	0.0155	0.059	0.084	0.0853	0.2564	0.2818
Std %	0.3221	3.8679	5.359	3.8812	7.1579	1.0078	0.9087	1.2032	3.6009	3.9074
MD %	-1.5242	-18.8729	-14.3885	-28.0879	-52.5689	-7.8581	-7.053	-11.1846	-21.592	-24.525
MD date	2020-11-30	2021-05-19	2021-01-08	2021-05-19	2020-12-23	2021-05-19	2021-05-19	2021-05-19	2021-05-19	2021-05-19

Table 4: First two moments, maximum dropdown (MD) and date fo MD of assets and hedge portfolios out-of-sample return.

robust HE result (instead of a point estimate), we apply the bootstrapping method. Bootstrapping refers to sampling from the empirical distribution of a given data sample (e.g. a time series of financial returns). The principal idea underlying bootstrapping is to provide statistical information about estimators that cannot be derived from just one realisation of the data. The method was introduced by Efron (1979); see also (Efron and Tibshirani, 1994; Davison and Hinkley, 1997).

A specific type of bootstrapping method designed for timeseries, namely the stationary block bootstrap Politis and Romano (1994), is applied in our analysis. The stationary bootstrapping procedure is as follows. Assume a time series $\{X_t\}_{t \in [1, N]}$ that is a stationary weakly time dependent time series, we first draw a block of samples $\{X_i, \dots, X_{i+j-1}\}$, where the index i is a random variable uniformly distributed over $[1, 2, \dots, N]$ and j is geometric distributed random variable with parameter p independent of i . For any index k which is greater than N , the sample X_k is defined to be $X_{k(\text{mod}N)}$. Then, we repeat the procedure until the number of samples are drawn in total across the blocks equal or exceed a predefined sample length S . One bootstrapped time series sample is then the concatenation of the blocks truncated to length of S . The resulting bootstrapped time series is known as pseudo time series.

We choose $p = 1/5$, implying the average block length is 5 such that it aligns with the recalibration frequency. The length of each pseudo time series sample $S = 300$ is chosen to be aligned with the length of each training set. The length of each pseudo time series sample allows ES and VaR to be calculated in a reasonable length. We draw in total $n = 500$ pseudo time series, for each of them we compute various HE measures to obtain a collection of HE samples.

Figure 12 reports the bootstrapped HE samples. As expected, the BTC involving spots, the BTC, CRIX, BITX and BITW100, are well hedged by the BTCF. The HEs of the other cryptos and indices are substantially lower than to the BTC-related instruments, but exhibit a consistent performances across different risk measures. As it turns out, some HE bootstrapping samples are even negative, which means the “hedge” portfolio actually increases the risk. This shows BTC futures is not suitable for cross-asset hedges (cross hedge). In fact, in the previous study by Corbet et al. (2018), researchers yield negative hedging effectiveness even when hedging against BTC exposure. show that derivatives in BitMEX

6 Conclusion and Outlook

We study the effectiveness of hedging cryptos and crypto indices with Bitcoin futures. To accommodate different risk appetites and scenarios, a variety of commonly used risk measures are considered to determine the optimal hedge ratio. The risk measures comprise variance, value-at-risk at the confidence levels 95% and 99%, expected shortfall 95% and 99%, and the exponential risk measure with parameter $k = 10$.

At the time of writing, the crypto market is a vibrant and fast-developing market, causing cryptos to have complex and time-changing dependence structures with the Bitcoin futures. As a consequence, the dependence between the cryptos and the futures contract plays an important role in hedging as it determines the distribution of the portfolio returns. We therefore consider various copulae, a flexible statistical tool that separates modelling of the marginals and the dependence structure of multivariate random vectors. To address the potential time-changing dependence, we periodically re-calibrate the copula models and determine the best-fitting copula via AIC.

An extensive out-of-sample backtest suggests that Bitcoin futures are consistently capable of hedging BTC and BTC-involved indices, i.e., BITX, CRIX, and BITW100, under different risk minimisation

objectives and copula models. The mean-square errors (MSEs) and lower semi-variances (LSVs) of the resulting portfolios are indistinguishable at a low level except for the Frank copula. For BTC-related spot asset, the AIC procedure consistently favours the t -copula because it captures the tail dependence feature of the data. Compared to the unhedged cases, the portfolios' out-of-sample maximum drawdowns are significantly reduced.

Contrarily, we observe more diverse results of the capability of BTC futures to hedge other cryptos and crypto indices that exclude Bitcoin. In general, ES 95% and VaR 95% perform better than their 99% in terms of mean square error (MSE) and lower semi variance (LSV). In particular, minimising ES 99% leads to relatively high MSEs and LSVs regardless of the copula in use. The ES 99% and VaR 99% even result in out-of-sample maximum drawdowns that are higher than that of the 95% counterparts in some portfolios, for example in the ETH- and LTC-BTCF portfolios. Therefore, we conclude that overly emphasising tail risks by choosing extreme tail risk measures does not lead to a promising hedge in a cross-hedging setting.

As an intermediate step in determining the optimal hedge ratio, the AIC procedure mainly favours the rotated Gumbel and the NIG factor copula in modelling non-BTC related cryptos and indices. This reflects the systematic nature of downward movements in the crypto market. Interestingly, the best-fitting copula does not necessary lead to the best performing portfolio in terms of MSE or LSV. This is the case, for example, for ADA. We suspect that this discrepancy between the optimal copula selection and MSE-LSV results can be attributed to the static linear nature of the hedge, as the sole hedge instrument is a futures contract; the hedge is not sophisticated enough to react to the more involved dependence structure.

With further analysis, the conclusion drawn from this study can also be applied to crypto market related policy making. Our results connect to the discussion of whether authority should allow crypto futures hedge as basis to lower the minimum capital requirements inflicted by crypto exposure. While the debates carry on at the time of writing, our results align and can be seen as an extension of the existing researches made by stakeholders, for example, research done by CME ⁹, and International Swaps and Derivatives Association's report ¹⁰. Nonetheless, further studies are required to rule out or understand the risks other than market risk, e.g. operation risk and counterparty risk.

On the other hand, our results provide partial evidences in supporting separate treatments of cryptos with a matured regulated derivatives market and those without. Our results show a clear distinction between the hedging effectiveness of BTC futures to BTC related assets and BTC unrelated assets. Hedgers are empowered by the BTC futures to manage their BTC and BTC-related exposure, but not the other crypto exposures. Further studies are required to generalise the hedging effectiveness of other crypto-futures pairs.

⁹See the CME and KPMG's reports on <https://www.cmegroup.com/education/files/basics-of-hedge-effectiveness.pdf>

¹⁰See the ISDA report "Crypto-asset Risks and Hedging Analysis" on <https://www.isda.org/a/pMWgE/Crypto-asset-Risks-and-Hedging-Analysis.pdf>

References

- (????): “REGULATION (EU) No 575/2013 OF THE EUROPEAN PARLIAMENT AND OF THE COUNCIL of 26 June 2013 on prudential requirements for credit institutions and investment firms and amending Regulation (EU) No 648/2012,” .
- ABRAMOWITZ, M. AND I. STEGUN (1964): *Handbook of Mathematical Functions with Formulas, Graphs, and Mathematical Tables*, Applied mathematics series, U.S. Government Printing Office, 1972.
- ACERBI, C. (2002): “Spectral measures of risk: A coherent representation of subjective risk aversion,” *Journal of Banking & Finance*, 26, 1505–1518.
- AKAIKE, H. (1973): “Information theory and an extension of the maximum likelihood principle,” in *Second International Symposium on Information Theory*, ed. by B. N. Petrov and F. Csaki, Budapest: Akadémiai Kiado, 267–281.
- ALEXANDER, C., J. CHOI, H. PARK, AND S. SOHN (2020): “BitMEX bitcoin derivatives: Price discovery, informational efficiency, and hedging effectiveness,” *Journal of Futures Markets*, 40, 23–43.
- ALEXANDER, C., J. DENG, AND B. ZOU (2021): “Hedging with bitcoin futures: The effect of liquidation loss aversion and aggressive trading,” *arXiv preprint arXiv:2101.01261*.
- ANDERSON, D., K. BURNHAM, AND G. WHITE (1998): “Comparison of Akaike information criterion and consistent Akaike information criterion for model selection and statistical inference from capture-recapture studies,” *Journal of Applied Statistics*, 25, 263–282.
- ARTZNER, P., F. DELBAEN, J.-M. EBER, AND D. HEATH (1999): “Coherent measures of risk,” *Mathematical Finance*, 9, 203–228.
- BARBI, M. AND S. ROMAGNOLI (2014): “A Copula-Based Quantile Risk Measure Approach to Estimate the Optimal Hedge Ratio,” *Journal of Futures Markets*, 34, 658–675.
- BARNDORFF-NIELSEN, O. E. (1997): “Normal inverse Gaussian distributions and stochastic volatility modelling,” *Scandinavian Journal of statistics*, 24, 1–13.
- BREYMAN, W., A. DIAS, AND P. EMBRECHTS (2003): “Dependence structures for multivariate high-frequency data in finance,” .
- CHERUBINI, U., S. MULINACCI, AND S. ROMAGNOLI (2011): “A copula-based model of speculative price dynamics in discrete time,” *Journal of Multivariate Analysis*, 102, 1047–1063.
- CONT, R. (2001): “Empirical properties of asset returns: stylized facts and statistical issues,” *Quantitative Finance*, 1, 223–236.
- CORBET, S., B. LUCEY, M. PEAT, AND S. VIGNE (2018): “Bitcoin Futures—What use are they?” *Economics Letters*, 172, 23–27.
- DAVISON, A. C. AND D. V. HINKLEY (1997): *Bootstrap methods and their application*, 1, Cambridge university press.

- DEMARTA, S. AND A. J. MCNEIL (2005): “The t copula and related copulas,” *International statistical review*, 73, 111–129.
- DENG, J., H. PAN, S. ZHANG, AND B. ZOU (2020): “Minimum-variance hedging of Bitcoin inverse futures,” *Applied Economics*, 52, 6320–6337.
- DOWD, K., J. COTTER, AND G. SORWAR (2008): “Spectral risk measures: properties and limitations,” *Journal of Financial Services Research*, 34, 61–75.
- EDERINGTON, L. H. (1979): “The hedging performance of the new futures markets,” *The journal of finance*, 34, 157–170.
- EFRON, B. (1979): “Bootstrap methods: another look at the jackknife,” *Annals of Statistics*, 1–26.
- EFRON, B. AND R. J. TIBSHIRANI (1994): *An introduction to the bootstrap*, CRC press.
- EMBRECHTS, P., A. MCNEIL, AND D. STRAUMANN (2002): “Correlation and dependence in risk management: properties and pitfalls,” *Risk management: value at risk and beyond*, 1, 176–223.
- FAMA, E. F. (1963): “Mandelbrot and the stable Paretian hypothesis,” *The Journal of Business*, 36, 420–429.
- FISHER, N. I. AND P. K. SEN (2012): *The collected works of Wassily Hoeffding*, Springer Science & Business Media.
- FÖLLMER, H. AND A. SCHIED (2002): *Stochastic Finance. An Introduction in Discrete Time*, de Gruyter.
- GENEST, C. (1987): “Frank’s family of bivariate distributions,” *Biometrika*, 74, 549–555.
- GENEST, C. AND L.-P. RIVEST (1993): “Statistical inference procedures for bivariate Archimedean copulas,” *Journal of the American statistical Association*, 88, 1034–1043.
- HÄRDLE, W. K., N. HAUTSCH, AND L. OVERBECK (2008): *Applied Quantitative Finance*, Springer Science & Business Media.
- HÄRDLE, W. K., M. MÜLLER, S. SPERLICH, AND A. WERWATZ (2004): *Nonparametric and Semiparametric Models*, Springer Science & Business Media.
- HÄRDLE, W. K. AND L. SIMAR (2019): *Applied multivariate statistical analysis Fifth Edition*, Springer.
- HOEFFDING, W. (1940a): “Masstabinvariante Korrelationstheorie,” *Schriften des Mathematischen Instituts und Instituts für Angewandte Mathematik der Universität Berlin*, 5, 181–233.
- (1940b): “Scale-invariant correlation theory (English translation),” 5, 181–233.
- (1941): “Scale-invariant correlations for discontinuous distributions (English translation),” 7, 49–70.
- JOE, H. (1997): *Multivariate models and multivariate dependence concepts*, CRC Press.
- (2014): *Dependence modeling with copulas*, CRC press.

- KALEMANOVA, A., B. SCHMID, AND R. WERNER (2007): “The normal inverse Gaussian distribution for synthetic CDO pricing,” *The Journal of Derivatives*, 14, 80–94.
- KRUPSKII, P., R. HUSER, AND M. G. GENTON (2018): “Factor copula models for replicated spatial data,” *Journal of the American Statistical Association*, 113, 467–479.
- KRUPSKII, P. AND H. JOE (2013): “Factor copula models for multivariate data,” *Journal of Multivariate Analysis*, 120, 85–101.
- MCNEIL, A., R. FREY, AND P. EMBRECHTS (2005): *Quantitative Risk Management*, Princeton, NJ: Princeton University Press.
- (2015): *Quantitative Risk Management*, Princeton, NJ: Princeton University Press, 2nd ed.
- MENEZES, C., C. GEISS, AND J. TRESSLER (1980): “Increasing downside risk,” *The American Economic Review*, 70, 921–932.
- NAKAMOTO, S. (2009): “Bitcoin: A Peer-to-Peer Electronic Cash System,” .
- NELSEN, R. (2002): “Concordance and copulas: A survey,” in *Distributions with Given Marginals and Statistical Modelling*, Kluwer Academic Publishers, 169–178.
- NELSEN, R. B. (1999): *An Introduction to Copulas*, Springer.
- OH, D. H. AND A. J. PATTON (2013): “Simulated method of moments estimation for copula-based multivariate models,” *Journal of the American Statistical Association*, 108, 689–700.
- POLITIS, D. N. AND J. P. ROMANO (1994): “The Stationary Bootstrap,” *Journal of the American Statistical Association*, 1303–1313.
- SCHWEIZER, B., E. F. WOLFF, ET AL. (1981): “On nonparametric measures of dependence for random variables,” *Annals of Statistics*, 9, 879–885.
- SEBASTIÃO, H. AND P. GODINHO (2020): “Bitcoin futures: An effective tool for hedging cryptocurrencies,” *Finance Research Letters*, 33, 101230.
- SKLAR, A. (1959): “Fonctions de répartition a n dimensions et leurs marges,” *Publications de l’Institut de Statistique de l’Université de Paris*, 8, 229–231.
- TAKEUCHI, K. (1976): “Distribution of informational statistics and a criterion of model fitting. Suri-Kagaku (Mathematical Sciences) 153 12-18,” .
- VIRTANEN, P., R. GOMMERS, T. E. OLIPHANT, M. HABERLAND, T. REDDY, D. COURNAPEAU, E. BUROVSKI, P. PETERSON, W. WECKESSER, J. BRIGHT, S. J. VAN DER WALT, M. BRETT, J. WILSON, K. J. MILLMAN, N. MAYOROV, A. R. J. NELSON, E. JONES, R. KERN, E. LARSON, C. J. CAREY, İ. POLAT, Y. FENG, E. W. MOORE, J. VANDERPLAS, D. LAXALDE, J. PERKTOLD, R. CIMRMAN, I. HENRIKSEN, E. A. QUINTERO, C. R. HARRIS, A. M. ARCHIBALD, A. H. RIBEIRO, F. PEDREGOSA, P. VAN MULBREGT, AND SCI-PY 1.0 CONTRIBUTORS (2020): “SciPy 1.0: Fundamental Algorithms for Scientific Computing in Python,” *Nature Methods*, 17, 261–272.
- ZEEVI, A. AND R. MASHAL (2002): “Beyond correlation: Extreme co-movements between financial assets,” *Available at SSRN 317122*.

A Density of linear combination of random variables

Proposition 3 *Let $\mathbf{X} = (X_1, \dots, X_d)^\top$ be real-valued random variables with corresponding copula density $\mathbf{c}_{X_1, \dots, X_d}$, and continuous marginals F_{X_1}, \dots, F_{X_d} . Then, the pdf of the linear combination of marginals $Z = n_1 \cdot X_1 + \dots + n_d \cdot X_d$ is*

$$f_Z(z) = |n_1^{-1}| \int_{[0,1]^{d-1}} \mathbf{c}_{X_1, \dots, X_d}(F_{X_1}(S(z)), u_2, \dots, u_d) \cdot f_{X_1}(S(z)) du_2 \dots du_d, \quad (8)$$

with

$$S(z) = \frac{1}{n_1} \cdot z - \frac{n_2}{n_1} \cdot F_{X_2}^{(-1)}(u_2) - \dots - \frac{n_d}{n_1} \cdot F_{X_d}^{(-1)}(u_d).$$

Proof. Let

$$\mathbf{A} = \begin{bmatrix} n_1 & n_2 & \dots & n_d \\ 0 & 1 & \dots & 0 \\ 0 & 0 & 1 & \dots & 0 \\ \vdots & & & \ddots & \vdots \\ 0 & \dots & & 1 & \end{bmatrix}.$$

Then,

$$\begin{bmatrix} Z \\ X_2 \\ \vdots \\ X_d \end{bmatrix} = \mathbf{A} \begin{bmatrix} X_1 \\ X_2 \\ \vdots \\ X_d \end{bmatrix}.$$

By transformation of the variables (Härdle and Simar, 2019, Section 4.3),

$$\begin{aligned} \mathbf{f}_{Z, X_2, \dots, X_d}(z, x_2, \dots, x_d) &= \mathbf{f}_{X_1, \dots, X_d} \left(\mathbf{A}^{-1} \begin{bmatrix} z \\ x_2 \\ \vdots \\ x_d \end{bmatrix} \right) \cdot |\det \mathbf{A}^{-1}| \\ &= |n_1^{-1}| \mathbf{f}_{X_1, \dots, X_d}(S(z), x_2, \dots, x_d). \end{aligned}$$

Let $u_i = F_{X_i}(x_i)$. By chain rule we have

$$\begin{aligned} \mathbf{f}_{X_1, \dots, X_d}(x_1, \dots, x_d) &= \frac{\partial^d F_{X_1, \dots, X_d}(x_1, \dots, x_d)}{\partial x_1 \dots \partial x_d} \\ &= \mathbf{c}_{X_1, \dots, X_d}(u_1, \dots, u_d) \cdot \prod_{i=1}^d f_{X_i}(x_i). \end{aligned}$$

Therefore,

$$\begin{aligned} \mathbf{f}_{Z, X_2, \dots, X_d}(z, x_2, \dots, x_d) &= \\ &= |n_1^{-1}| \cdot \mathbf{c}_{X_1, \dots, X_d}(F_{X_1}(S(z)), u_2, \dots, u_d) \cdot f_{X_1}\{S(z)\} \cdot \prod_{i=2}^d f_{X_i}(x_i). \end{aligned}$$

The claim (8) is obtained by integrating out x_2, \dots, x_d by substituting $dx_i = \frac{1}{f_{X_i}(x_i)} du_i$. ■

B Summary Statistics

	Mean %	Std %	Skew	Kurt	MD %	MD date	ρ	τ
Hedging Instrument								
BTCTF	0.3906	4.6312	-0.5060	4.4204	-26.9920	2020-03-12	1.0000	1.0000
Individual Cryptos								
BTC	0.3915	4.4023	-0.5857	4.6565	-25.9965	2020-03-12	0.9975	0.9507
ETH	0.6819	6.0103	-0.2557	5.2646	-32.0144	2020-03-12	0.7712	0.5988
ADA	0.9467	6.6990	0.1661	2.3086	-26.8528	2020-03-12	0.6296	0.4825
LTC	0.3227	6.4781	-0.9935	5.3011	-37.5913	2021-05-19	0.8080	0.6113
XRP	0.2987	7.9843	0.5542	12.4882	-52.7652	2020-12-23	0.4510	0.4939
Crypto Indices with BTC Constituent								
BITX	0.4308	4.5676	-0.8842	4.7222	-27.0220	2020-03-12	0.9769	0.8738
CRIX	0.4602	4.5420	-0.7952	4.7549	-27.1385	2020-03-12	0.9799	0.8769
BITW100	0.4683	4.6174	-0.9864	4.9381	-27.2694	2020-03-12	0.9674	0.8537
Crypto Indices without BTC Constituent								
BITW20	0.6249	5.5021	-1.1518	5.2203	-31.0092	2020-03-12	0.7674	0.5883
BITW70	0.6353	5.8155	-1.1171	5.1926	-32.3453	2021-05-19	0.7525	0.5459

Table 5: Summary statistics of assets' daily returns during the out-of-sample period, from 2019-10-21 to 2021-05-27. The first four columns are the first four moments of assets' daily returns. The fifth and sixth columns are the maximum drawdown (MD) and the date of the MD. The last two columns are Pearson's ρ s and Kendall's τ s between the assets and BTCTF.

	Mean %	Std %	Skew	Kurt	MD %	MD date	Variance
Individual Cryptos							
BTC	0.0215	0.3221	-1.0119	3.1929	-1.4393	2020-11-30	0.0000
ETH	0.2823	3.8741	0.9469	7.1064	-17.7421	2021-05-19	0.0015
ADA	0.5617	5.2722	1.3634	4.4818	-13.8687	2021-01-08	0.0028
LTC	-0.0871	3.9052	-0.3617	7.6239	-28.3029	2021-05-19	0.0018
XRP	-0.0123	7.1537	1.1451	20.0236	-52.5236	2020-12-23	0.0043
Crypto Indices with BTC Constituent							
BITX	0.0561	0.9954	-0.4204	13.2487	-7.7567	2021-05-19	0.0001
CRIX	0.0812	0.9183	-0.0027	14.3136	-7.1025	2021-05-19	0.0001
BITW100	0.0855	1.1986	-1.7440	22.2644	-11.3866	2021-05-19	0.0001
Crypto Indices without BTC Constituent							
BITW20	0.2429	3.5846	-0.3063	4.1622	-21.4680	2021-05-19	0.0013
BITW70	0.2706	3.8838	-0.6490	4.6312	-23.9984	2021-05-19	0.0015

Table 6: Summary statistics of out-of-sample daily returns of hedged portfolios that minimize variance.

	Mean %	Std %	Skew	Kurt	MD %	MD date	VaR 5%
Individual Cryptos							
BTC	0.0253	0.3294	-0.9725	3.4373	-1.5347	2020-11-30	0.0063
ETH	0.3084	3.8944	1.0243	7.4297	-19.1750	2021-05-19	0.0514
ADA	0.5726	5.2204	1.2981	4.2544	-14.6974	2021-05-19	0.0769
LTC	-0.0742	3.9145	-0.3836	7.5384	-28.3672	2021-05-19	0.0622
XRP	0.0208	7.1520	1.1269	19.8930	-52.5667	2020-12-23	0.0683
Crypto Indices with BTC Constituent							
BITX	0.0562	0.9930	-0.3117	12.4780	-7.5639	2021-05-19	0.0128
CRIX	0.0863	0.9151	0.0718	13.7915	-6.9744	2021-05-19	0.0092
BITW100	0.0846	1.1980	-1.6592	21.3725	-11.2582	2021-05-19	0.0164
Crypto Indices without BTC Constituent							
BITW20	0.2728	3.5940	-0.3721	4.4896	-22.0733	2021-05-19	0.0546
BITW70	0.2847	3.9133	-0.6580	4.7874	-24.6513	2021-05-19	0.0626

Table 7: Summary statistics of out-of-sample daily returns of hedged portfolios that minimize VaR 5%.

	Mean %	Std %	Skew	Kurt	MD %	MD date	VaR 1%
Individual Cryptos							
BTC	0.0176	0.3270	-1.0405	3.3742	-1.5689	2020-11-30	0.0134
ETH	0.2977	3.9132	0.9547	7.2414	-18.6061	2021-05-19	0.1026
ADA	0.5562	5.3466	1.1362	3.9334	-15.4795	2021-05-19	0.1106
LTC	-0.0852	4.1503	-0.7234	7.3208	-29.0915	2021-05-19	0.1030
XRP	0.0352	7.1658	1.1582	19.8506	-52.5727	2020-12-23	0.1387
Crypto Indices with BTC Constituent							
BITX	0.0593	1.0178	-0.5331	13.3100	-8.0299	2021-05-19	0.0247
CRIX	0.0738	0.9695	-0.4729	13.6500	-7.0185	2021-05-19	0.0245
BITW100	0.0823	1.2338	-1.9365	23.1938	-11.8752	2021-05-19	0.0347
Crypto Indices without BTC Constituent							
BITW20	0.2499	3.6210	-0.3866	4.3396	-21.6634	2021-05-19	0.0988
BITW70	0.2788	3.9257	-0.7635	5.1288	-24.5294	2021-05-19	0.1147

Table 8: Summary statistics of out-of-sample daily returns of hedged portfolios that minimize VaR 1%.

	Mean %	Std %	Skew	Kurt	MD %	MD date	ES 5%
Individual Cryptos							
BTC	0.0204	0.3234	-1.0150	3.4423	-1.5629	2020-11-30	0.0101
ETH	0.3082	3.8890	1.0119	7.4077	-18.7819	2021-05-19	0.0782
ADA	0.5525	5.2673	1.2557	4.2423	-14.9647	2021-05-19	0.0984
LTC	-0.0808	3.9829	-0.4957	7.2302	-28.4608	2021-05-19	0.0962
XRP	0.0176	7.1533	1.1411	19.9176	-52.5698	2020-12-23	0.1354
Crypto Indices with BTC Constituent							
BITX	0.0591	1.0065	-0.3453	12.1335	-7.6211	2021-05-19	0.0215
CRIX	0.0777	0.9207	0.0164	13.5608	-6.9894	2021-05-19	0.0173
BITW100	0.0848	1.2125	-1.6397	19.7472	-11.1357	2021-05-19	0.0274
Crypto Indices without BTC Constituent							
BITW20	0.2608	3.6115	-0.3555	4.2016	-21.5430	2021-05-19	0.0804
BITW70	0.2785	3.9157	-0.6949	4.8047	-24.3474	2021-05-19	0.0908

Table 9: Summary statistics of out-of-sample daily returns of hedged portfolios that minimize ES 5%.

	Mean %	Std %	Skew	Kurt	MD %	MD date	ES 1%
Individual Cryptos							
BTC	0.0148	0.3476	-0.8354	3.3054	-1.6225	2020-11-30	0.0234
ETH	0.3080	3.8954	0.9840	7.4947	-18.7625	2021-05-19	0.1299
ADA	0.5016	5.4040	1.1008	3.9607	-15.4481	2021-05-19	0.1463
LTC	-0.1029	4.1581	-0.7757	7.4375	-29.1727	2021-05-19	0.1647
XRP	-0.0200	7.2887	1.1121	18.8732	-52.5700	2020-12-23	0.2516
Crypto Indices with BTC Constituent							
BITX	0.0598	1.0312	-0.4410	11.5863	-7.7424	2021-05-19	0.0411
CRIX	0.0835	0.9461	-0.0361	12.4047	-7.0203	2021-05-19	0.0350
BITW100	0.0781	1.2640	-1.9645	21.8836	-11.9263	2021-05-19	0.0593
Crypto Indices without BTC Constituent							
BITW20	0.2538	3.6323	-0.4086	4.4462	-21.9866	2021-05-19	0.1282
BITW70	0.2660	3.9320	-0.7598	5.0050	-24.4764	2021-05-19	0.1535

Table 10: Summary statistics of out-of-sample daily returns of hedged portfolios that minimize ES 1%.

	Mean %	Std %	Skew	Kurt	MD %	MD date	ERM k=10
Individual Cryptos							
BTC	0.0223	0.3221	-1.0008	3.4153	-1.5242	2020-11-30	0.0057
ETH	0.3117	3.8679	1.0345	7.5751	-18.8729	2021-05-19	0.0491
ADA	0.5722	5.3590	1.4203	4.6970	-14.3885	2021-01-08	0.0700
LTC	-0.0512	3.8812	-0.2929	7.7022	-28.0879	2021-05-19	0.0616
XRP	0.0155	7.1579	1.1244	19.8583	-52.5689	2020-12-23	0.0787
Crypto Indices with BTC Constituent							
BITX	0.0590	1.0078	-0.4427	13.0839	-7.8581	2021-05-19	0.0127
CRIX	0.0840	0.9087	0.0488	14.5501	-7.0530	2021-05-19	0.0100
BITW100	0.0853	1.2032	-1.6522	20.5562	-11.1846	2021-05-19	0.0153
Crypto Indices without BTC Constituent							
BITW20	0.2564	3.6009	-0.3446	4.2152	-21.5920	2021-05-19	0.0503
BITW70	0.2818	3.9074	-0.6952	4.8745	-24.5250	2021-05-19	0.0557

Table 11: Summary statistics of out-of-sample daily returns of hedged portfolios that minimize ERM $k = 10$.

C Supplementary Material: Intraday Hedging

Here we extend the hedging effectiveness analysis to intraday data again through backtesting. BTC and ETH are chosen as spot to be hedged against by BTCF. The backtesting procedure in this section is the same to that of the main body, except the followings:

1. recalibration and rebalancing frequency are increased to every 4 hours,
2. lengths of training data and test data are changed to 336 (equivalent to 14 days) and 4 respectively, and
3. the stationary bootstrapping parameters are changed to $p = 1/4, T = 336, S = 1000$ to adapt to the new rebalancing frequency.

The increased recalibration and rebalancing frequency require data with higher granularity that CME does not provide, forcing us to backtest with data from other crypto exchanges.

We collect price data from Deribit from 2020-06-01 00:00 UTC to 2020-08-01 00:00 UTC. All price data are hourly data. The Deribit contract BTC-25SEP20 represents BTCF; the Deribit BTC and ETH index represent the spot of BTC and ETH, respectively. We take the hourly closing mid-price of the BTC-25SEP20 as the futures price and the last value of the BTC and ETH index in every hourly bucket as the spot prices. Since the date range of the data is fully covered by the lifetime of BTC-25SEP20, this study does not require futures contract rollover.

Note that the exact values of MSE, LSV or HE from the two rebalancing schedules shall not be directly compared for two reasons: 1. The data are from different date ranges; 2. Various factors contribute to the difference between two sampling frequencies, e.g. Epps effect, microstructure noise, and asynchronous trading. However, we compare the patterns and conclusions of the two to get a general understanding of the hedging issue for future use.

Figure 13 presents the bootstrapped out-of-sample HEs. In general, the daily rebalancing results of BTC-BTCF carry over to the intraday rebalancing schedule; The intraday rebalancing ETH-BTCF is different from its daily rebalancing counterpart. The main difference between the intraday rebalancing and daily rebalancing ETH-BTCF portfolio is that negative HEs appear in the intraday results in all the risk measures we consider. This implies that hedgers cannot gain hedging potential from intraday dependence between BTC and ETH to hedge an ETH crypto position.

Turning to BTC-BTCF, the HEs of BTC-BTCF are significantly higher than zero across different risk measures, suggesting that adding BTCF to a BTC portfolio can effectively reduce the risk measured by selected measures. Among risk measures, HE of variance is the highest, ranging between 72% to 98%, while the HE's other risk measures range between 25% to 80%. Reducing variance being a well-achievable objective is consistent with the findings of the daily rebalancing schedule. On the other hand, the HEs of ES99% and VaR99% are relatively more dispersed and skewed to the left. Both risk measures consider only 1% of the data from the left for deciding the hedge ratio and computing the HEs. Considering only a few data points naturally leads to a less reliable hedge ratio and lower consistency HEs. Evidence also shows that ES99% VaR99% minimising portfolios have higher MSE and LSV. This result is again consistent with the daily rebalancing setting.

Figures 14 and 15 report the out-of-sample MSE and LSV of the BTC-BTCF when different copulae and risk measures are in use. The MSEs and LSVs share similar patterns to that of the daily rebalancing setting. Across various copulae, the BTC-BTCF portfolio that minimises VaR95% provides the lowest MSE and LSV. Portfolios that minimise variance and ERM with $k = 10$ are close

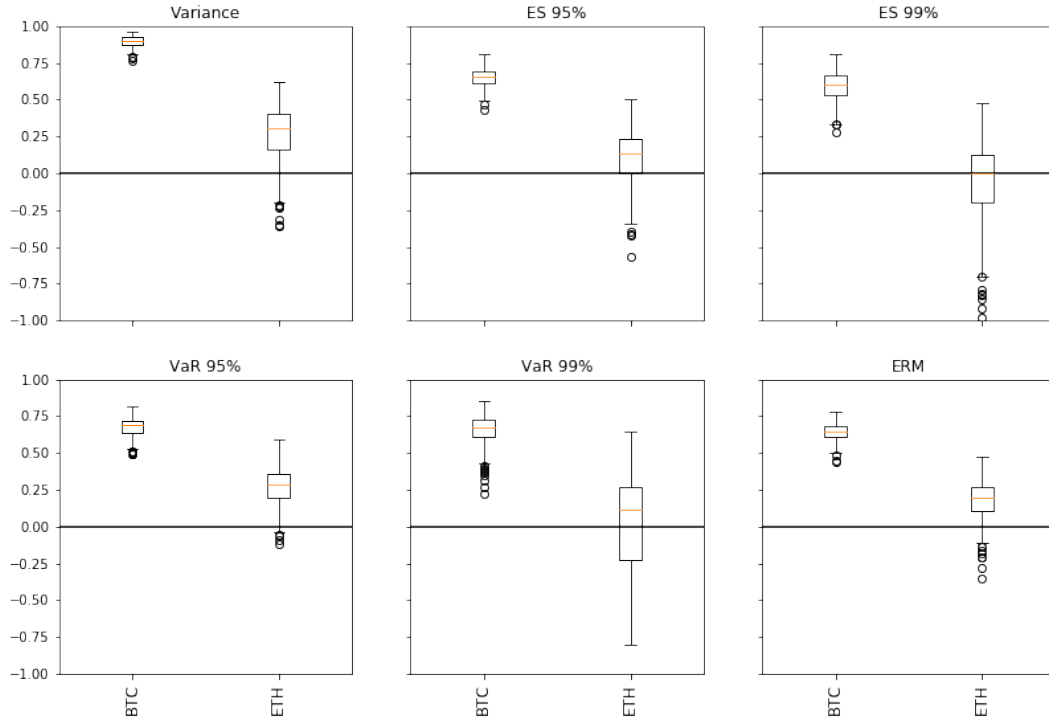



Figure 13: Intraday HEs of BTC-BTCF and ETH-BTCF portfolio. The HEs of BTC-BTCF portfolios are significantly higher than 0, which suggests involving the BTCF in the portfolio can effectively reduce market risk. The HEs of ETH-BTCF portfolios are lower than that of BTC-BTCF portfolios, and sometimes go below 0. We nullify the hedging ability of BTCF in this intraday ETH-BTCF setting. 

in MSEs and LSVs, The MSEs and LSVs are slightly higher than that of VaR95%, especially when Gumbel and NIG copulae are in use to model the dependence. ES99% generates the highest MSEs and LSVs, regardless of the copula.

Across various risk measures, Gumbel and NIG copulae perform well in the resulting portfolios' MSE and LSV, except for ES99%. The Frank copula performs worst, regardless of the risk measure. These results are consistent with the daily rebalancing setting and conclusion drawn in Barbi and Romagnoli (2014, p.667).

Table 12 shows the relative frequencies of the best fitting copula according to AIC. They are t -, Plackett, Gaussian Mix Independent, rotated Gumbel and NIG. Similar to the result in the daily rebalancing schedule, most of the time the AIC procedure chooses t -Copula to model the dependence structure of BTC-BTCF in the intraday setting. For the rest of the time, the NIG copula is mainly chosen. Rotated Gumbel, Gaussian Mix Independent, and Plackett are spontaneously chosen. On the other hand, the intraday ETH-BTCF's AIC selection result is very different from that of the daily rebalancing. There are three copulae: t -, Gaussian Mix Independent, and NIG copula, that are closely chosen, instead of a single copula, rotated Gumbel copula, dominating the list in the daily rebalancing setting.

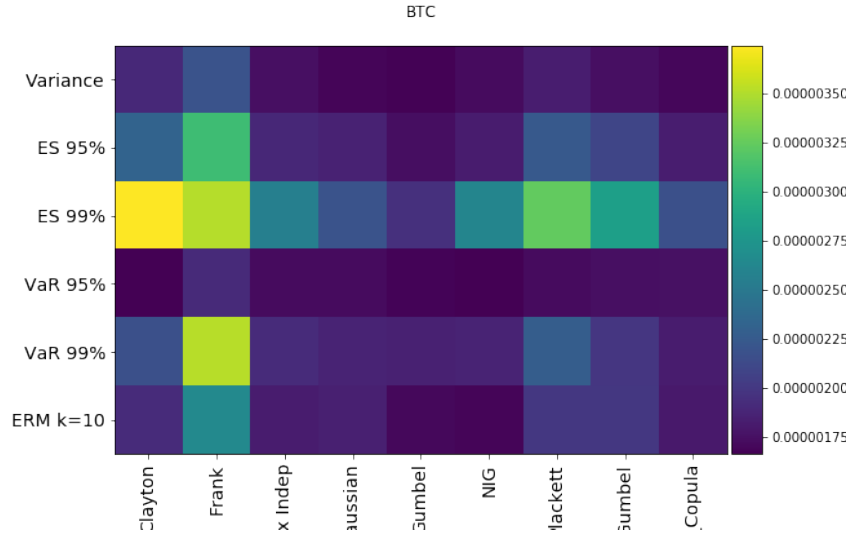


Figure 14: Intraday out-of-sample MSEs of the BTC-BTCF portfolio constructed by combinations of copula and ris minimization objectives. The Frank copula is again inferior. Minimising ES99% results in higher MSEs disregard of which copula is in use.  [Graph is cut off. Make pdf or eps.]

Spot/ Copula	t	Plackett	GMI	rotGumbel	NIG
BTC	60.00	1.11	3.33	8.89	26.67
ETH	35.14	0	24.32	15.68	24.86

Table 12: Intraday copula selection results (shortened). The values are the percentage counts of a copula chosen by the AIC procedure during the out-of-sample period. The table shows only the frequently chosen copula, i.e. t , Plackett, Gaussian Mix Independent (GMI), rotated Gumbel (rotGumbel), and Normal Inverse Gaussian factor copula (NIG).

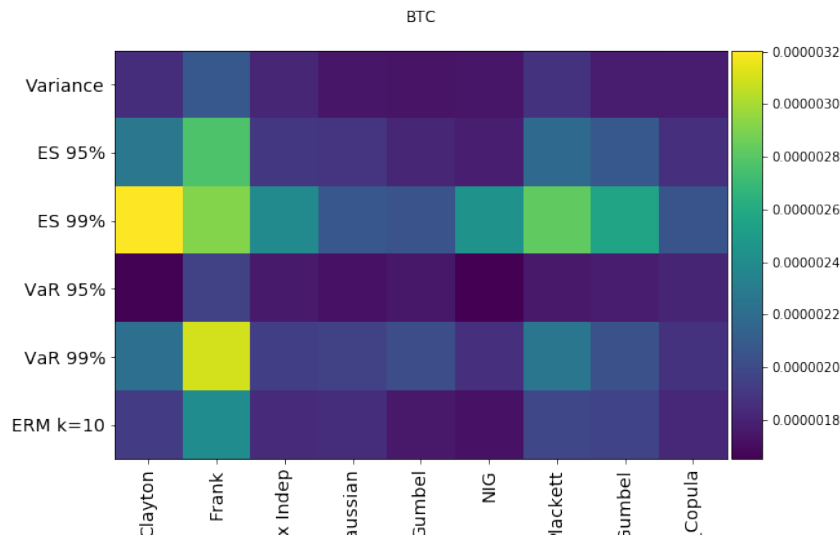


Figure 15: Intraday out-of-sample LSVs of the BTC-BTCF portfolio constructed by combinations of copula and ris minimization objectives. The Frank copula is again inferior. Minimising ES99% results in higher MSEs disregard of which copula is in use. 